Inorganic Chemistry

Article

pubs.acs.org/IC

Synthesis, Magnetic Properties, and Phosphoesterase Activity of Dinuclear Cobalt(II) Complexes

Lena J. Daumann,[†] Peter Comba,[‡] James A. Larrabee,[∥] Gerhard Schenk,[†,⊥] Robert Stranger,[§] German Cavigliasso,[§] and Lawrence R. Gahan*[,†]

[†]School of Chemistry and Molecular Biosciences, The University of Queensland, Brisbane QLD 4072, Australia

[‡]Anorganisch-Chemisches Institut, Universität Heidelberg, Im Neuenheimer Feld 270, 69120 Heidelberg, Germany

[§]Research School of Chemistry, Australian National University, Canberra 0200, Australia

[∥]Department of Chemistry and Biochemistry, Middlebury College, Middlebury, Vermont 05753, United States

[⊥]Department of Chemistry, National University of Ireland—Maynooth, Maynooth, Co. Kildare, Ireland

Supporting Information

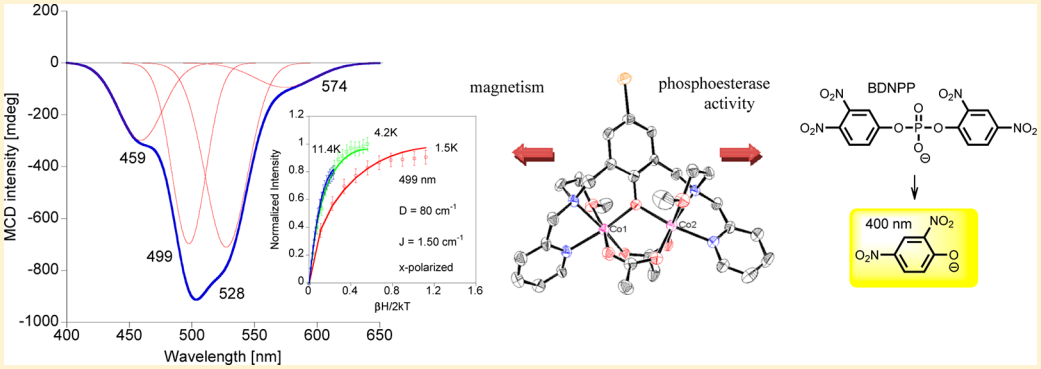

ABSTRACT: A series of dinuclear cobalt(II) complexes has been prepared and characterized to generate functional and spectroscopic models for cobalt(II) substituted phosphoesterase enzymes such as the potential bioremediator GpdQ. Reaction of ligands based on 2,2′-(((2-hydroxy-5-methyl-1,3-phenylene)bis(methylene))bis((pyridin-2-ylmethyl)azanediyl)))diethanol (**L1**) and 2,6-bis(((2-methoxyethyl)(pyridin-2-ylmethyl)amino)methyl)-4-methylphenol (**L2**) with cobalt(II) salts afforded $[Co_2(CO_2EtH_2\mathbf{L1})(CH_3COO)_2](PF_6)$, $[Co_2(CO_2Et\mathbf{L2})(CH_3COO)_2](PF_6)$, $[Co_2(CH_3\mathbf{L2})(CH_3COO)_2](PF_6)$, $[Co_2(Br\mathbf{L2})(CH_3COO)_2](PF_6)$, and $[Co_2(NO_2\mathbf{L2})(CH_3COO)_2](PF_6)$. Complexes of the **L2** ligands contain a coordinated methyl-ether, whereas the **L1** ligand contains a coordinated alcohol. The complexes were characterized using mass spectrometry, microanalysis, X-ray crystallography, UV−vis−NIR diffuse reflectance spectroscopy, IR absorption spectroscopy, solid state magnetic susceptibility measurements, and variable-temperature variable-field magnetic circular dichroism (VTVH MCD) spectroscopy. Susceptibility studies show that $[Co_2(CO_2EtH_2\mathbf{L1})(CH_3COO)_2](PF_6)$, $[Co_2(CO_2Et\mathbf{L2})(CH_3COO)_2](PF_6)$, and $[Co_2(CH_3\mathbf{L2})(CH_3COO)_2](PF_6)$ are weakly antiferromagnetically coupled, whereas $[Co_2(Br\mathbf{L2})(CH_3COO)_2](PF_6)$ and $[Co_2(NO_2\mathbf{L2})(CH_3COO)_2](PF_6)$ are weakly ferromagnetically coupled. The susceptibility results are confirmed by the VTVH MCD studies. Density functional theory calculations revealed that magnetic exchange coupling occurs mainly through the phenolic oxygen bridge. Implications of geometry and ligand design on the magnetic exchange coupling will be discussed. Functional studies of the complexes with the substrate bis(2,4-dinitrophenyl) phosphate showed them to be active towards hydrolysis of phosphoester substrates.

INTRODUCTION

The role of cobalt biomimetics in the elucidation of structure, spectroscopy, and mechanism of metalloenzymes, particularly in hydrolytic systems, is an active area of study. In early studies cobalt(III) complexes with ammine, macrocyclic, and tripodal amine ligands were employed as both structural and functional models of metallophosphatases.[1−7] The role of a coordinated hydroxide ion in these cobalt(III) systems was also investigated extensively.[1−9] There are examples of cobalt(II) complexes as phosphoesterase mimics.[10−15] The advantages of the spectroscopic and magnetic properties of cobalt(II) mimics, compared to those of cobalt(III) systems, are enhanced by the fact that cobalt(II) is frequently used to reconstitute enzyme activity, and that the vast majority of Co(II) substituted Zn(II) enzymes are hyperactive compared to the Zn(II)-form.[16] Of the available probes for cobalt(II), magnetic susceptibility and magnetic circular dichroism (MCD) spectroscopy have been shown to be

Received: November 6, 2012
Published: February 1, 2013

   dx.doi.org/10.1021/ic302418x | *Inorg. Chem.* 2013, 52, 2029−2043

Chart 1. Ligands Used To Mimic the Active Site Residues of GpdQ

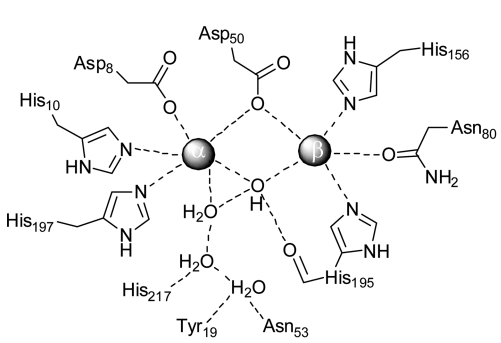

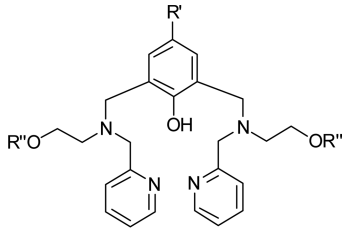

CO_2EtH_3L1 R' = CO_2Et, R" = H
CO_2EtHL2 R' = CO_2Et, R" = CH_3
CH_3HL2 R' = CH_3, R" = CH_3
BrHL2 R' = Br, R" = CH_3
NO_2HL2 R' = NO_2, R" = CH_3

useful to investigate the magnetic, geometric, and electronic structure of biologically relevant metal complexes.[17−20]

Herein, we report a continuation of our previous studies with zinc(II) and cadmium(II) biomimetic systems[21−23] as models of a glycerophosphodiesterase enzyme (GpdQ) from *Enterobacter aerogenes*.[18,24−28] We report a series of cobalt(II) complexes prepared from ligands based on the 2,2′-(((2-hydroxy-5-methyl-1,3-phenylene)bis(methylene))bis((pyridin-2-ylmethyl)azanediyl))diethanol[29] and 2,6-bis(((2-methoxyethyl)(pyridin-2-ylmethyl)amino)methyl)-4-methylphenol[21] frameworks with a range of substituents (CO_2Et-, NO_2-, Br-) replacing the CH_3- *para*- to the phenolic −OH in the parent ligands (Chart 1). The cobalt(II) complexes have been structurally characterized with X-ray crystallography, and the magnetic and spectroscopic properties have been investigated using variable-temperature variable-field (VTVH) MCD spectroscopy and solid-state magnetic susceptibility measurements. Density functional theory (DFT) calculations (broken symmetry approach) have been conducted to confirm the interpretation of the magnetic coupling constants obtained. In addition, functional studies have been undertaken with the substrate bis(2,4-dinitrophenyl)phosphate.

MATERIALS AND METHODS

General Methods. Positive-ion electrospray mass spectrometry was carried out with a Q-Star time-of-flight mass spectrometer, and the data were processed with Bruker Compass Data Analysis 4.0 software. FT-IR spectroscopy was carried out with a Perkin-Elmer FT-IR spectrometer SPECTRUM 2000 with a Smiths DuraSamplIR II ATR diamond window. Elemental microanalyses (C, H, N) were performed with a Carlo Erba elemental analyzer, model NA1500, by Mr. George Blazak at the University of Queensland. Phosphatase activity measurements were conducted with bis(2,4-dinitrophenol)phosphate (BDNPP) as substrate using a Varian Cary50 Bio UV−vis spectrophotometer with a Peltier temperature controller and 10-mm quartz cuvettes. The initial-rate method was employed, and assays were measured such that the initial linear portion of the data was used for analysis. Product formation was determined at 25 °C by monitoring the formation of 2,4-dinitrophenol. Throughout the pH range studied (4.75−11), the extinction coefficient of this product at 400 nm is 12 100 M^{-1} cm^{-1}.[30] All assays were measured in 50/50 acetonitrile/buffer with the substrate and complex initially dissolved in acetonitrile. The aqueous multicomponent buffer was composed of 50 mM 2-(*N*-morpholino)ethanesulfonic acid (MES, pH 5.50−6.50), 4-(2-hydroxyethyl)-1-piperazineethanesulfonic acid (HEPES, pH 7.00−8.50), 2-(*N*-cyclohexylamino)ethane sulfonic acid (CHES, pH 9.00−10.00), and *N*-cyclohexyl-3-aminopropanesulfonic acid (CAPS, pH 10.5−11) with controlled ionic strength ($LiClO_4$) 250 mM. The pH values reported are those of the aqueous component; it should however be noted that the pH of a solution of the buffer was the same within error as a 1:1 mixture of buffer and acetonitrile.[31] Assays for pH dependence were 40 μM in complex and 5 mM in BDNPP; for substrate dependence they were 40 μM in complex and 1−11.5 mM in BDNPP. pH-dependence data for monoprotic events were fit to the following equation.[32]

$$v_0 = \frac{V_{max}}{1 + \frac{[H^+]}{K_a}} \quad (1)$$

The data derived from substrate dependence were fit to the Michaelis−Menten equation.[32]

$$v = \frac{V_{max}[S]}{K_m + [S]} \quad (2)$$

Here, v is the initial rate, V_{max} is the maximum rate, K_m is the Michaelis constant, and $[S]$ is the substrate concentration. Complex dependence was measured with a fixed substrate concentration at 5 mM and complex concentrations ranging from 20 to 120 μM. Background assays were conducted by measuring the autohydrolysis and hydrolysis by 2 equiv of cobalt(II) acetate and were subtracted from the data.

Computational Methods. All calculations were performed with the Amsterdam Density Functional (ADF) package,[33−35] and the results reported were obtained using the 2010 version. Functionals based on the Generalized Gradient Approximation (GGA)[36,37] and hybrid methodology,[38−40] and basis sets of the all-electron type,[41] were used. In the present work we have carried out full geometry optimizations using pure density functional theory, and we have also performed additional calculations using hybrid methods. Relativistic effects were included by means of the Zero Order Regular Approximation (ZORA)[42−44] and the Conductor-like Screening Model (COSMO) was used for the treatment of solvation effects,[45] with ethanol as the solvent.

Crystallographic Measurements. Crystallographic data for the complexes were collected unless otherwise stated at 293(2) K with an Oxford Diffraction Gemini Ultra dual source (Mo and Cu) CCD diffractometer with Mo ($\lambda_{K\alpha}$ = 0.710 73 Å) or Cu ($\lambda_{K\alpha}$ = 1.5418 Å) radiation. The structures were solved by direct methods (SIR-92) and refined (SHELXL 97) by full matrix least-squares methods based on F^2.[46] These programs were accessed through the WINGX 1.70.01 crystallographic collective package.[47] All non-hydrogen atoms were refined anisotropically unless they were disordered. Hydrogen atoms were fixed geometrically and were not refined. X-ray data of the published structures were deposited with the Cambridge Crystallographic Data Centre, CCDC903307−903310.

Magnetic Susceptibility Measurements. Solid state susceptibility data were collected with a MPMS-XL 5T superconducting quantum interference device (SQUID) from Quantum Design at the University of Heidelberg, Germany,

dx.doi.org/10.1021/ic302418x | *Inorg. Chem.* 2013, 52, 2029−2043

and recorded as a function of the applied field (0−5 T), and at temperatures ranging from 2 to 300 K (zero field cooled method). The powdered samples were pressed into a PTFE band to avoid field-induced orientation of the powder and incorporated into two plastic straws as sample holder. The data were corrected for the diamagnetism of the PTFE band and sample holder; Pascal constant corrections for each sample were applied.[48] The program MagSaki was used for the analysis of magnetic susceptibility data.[49]

Diffuse Reflectance Spectroscopy. Spectra were measured at Middlebury College, VT, using a Varian Cary 6000i and a Purged Praying Mantis Diffuse Reflection Attachment (Harrick). Diffuse reflectance spectra were measured with magnesium oxide as blank and carrier material. The finely powdered samples were mixed (~1:1) with magnesium oxide and placed in the sample holder.

Magnetic Circular Dichroism (MCD). MCD measurements were conducted at Middlebury College, VT. Complex samples were both measured as solid mulls (poly(dimethylsiloxane)) and as saturated ethanol solutions. The MCD system used has a JASCO J815 spectropolarimeter and an Oxford Instruments SM4000 cryostat/magnet. Data were collected at increments of 0.5 Tesla (T) from 0 to 7.0 T and at temperatures of 1.4, 4.2, 11.3, 26, and 50 K. Each spectrum was corrected for any natural CD by subtracting the zero-field spectrum of the sample. Even when no sample is present, the instrument baseline exhibits a small deviation from zero that is both field- and wavelength-dependent. Therefore, each spectrum was also corrected by subtracting a spectrum recorded at the same magnetic field but with no sample present. The MCD spectra were fitted to the minimum number of Gaussian peaks using GramsAI 8.0 software after converting the spectra to wavenumber units.[50] In the fitting process the bandwidths of the d−d transitions were restrained to lie between 600 and 1000 cm^{-1}, and a minimum of Gaussians were fitted to achieve a satisfactory composite spectrum. The fitting of the VTVH MCD data was achieved using a locally written Fortran program, VTVH 2.1.1.[51] The spin Hamiltonian and additional details of the fitting program have been described previously.[19] The g values obtained by the SQUID measurements were used and fixed in fitting of the VTVH MCD data. In general, the initial values for D and J were those obtained from the SQUID measurements. In a general run, those values were fixed at first and then allowed to float one after the other to achieve a satisfactory fit. The fits were also tested for robustness once a complete set of parameters had been obtained. To do this, the initial parameters were set to the best fit parameters and then all allowed to float. Subsequently, one key parameter such as J, D, M_{xy}, M_{xz}, M_{yz} was chosen, its initial value was set differently, and the fit process was repeated. The rhombic zero field splitting parameter E was shown to have no effect on the VTVH fits, so E/D was set to zero in all fits (general convention $0 \leq E/D \leq {}^1/_3$). Percent polarization for a given fitted band was calculated from M_{xy}, M_{yz}, and M_{xz} using $\%M_x = (M_{xy}\cdot M_{xz})^2/[(M_{xy}\cdot M_{xz})^2 + (M_{xy}\cdot M_{yz})^2 + (M_{xz}\cdot M_{yz})^2]$. M_y and M_z were calculated correspondingly.[52] Finally, the VTVH MCD data fitting program used the Hamiltonian $H = -2JS_1S_2$, so the J values from VTVH MCD data fitting were converted to be comparable with those obtained by DFT calculations and magnetic susceptibility measurements.

Ligand Syntheses. Ethyl-4-hydroxy-3,5-bis(hydroxymethyl)benzoate, ethyl-3,5-bis(bromomethyl)-4-hydroxybenzoate, 2,6-bis(bromomethyl)-4-nitrophenol, 4-bromo-2,6-bis(hydroxymethyl)phenol, 2,6-bis(chloromethyl)-4-methylphenol, 2-methoxy-*N*-(pyridin-2-ylmethyl)-aminoethanol, *N*-(2-pyridylmethyl)-2-aminoethanol, ethyl-4-hydroxy-3,5-bis(((2-hydroxyethyl)(pyridin-2-ylmethyl)amino)-methyl)benzoate (CO_2EtH_3**L1**), ethyl-4-hydroxy-3,5-bis(((2-methoxyethyl)(pyridin-2-ylmethyl)amino)methyl)benzoate (CO_2EtH**L2**), 2,6-bis(((2-methoxyethyl)(pyridin-2-ylmethyl)-amino)methyl)-4-methylphenol (CH_3H**L2**), 4-bromo-2,6-bis-(((2-methoxyethyl)(pyridin-2-ylmethyl)amino)methyl)phenol (Br**HL2**), and 2,6-bis(((2-methoxyethyl)(pyridin-2-ylmethyl)-amino)methyl)-4-nitrophenol (NO_2H**L2**) were synthesized as described previously.[21−23]

Synthesis of $[Co_2(CO_2EtH_2L1)(CH_3COO)_2](PF_6)$. A methanol solution of CO_2EtH_3**L1** (0.1 M, 1 mL) was combined with a solution of cobalt(II) acetate tetrahydrate (0.1 M, 2 mL) in methanol. Subsequently, solid sodium hexafluorophosphate (50 mg, 0.3 mmol) was added. The pink solution was filtered and left to evaporate in air for 3 days to yield pink needles that were suitable for X-ray crystallography (88% yield). Microanalysis $C_{31}H_{39}Co_2N_4O_9PF_6$ requires: C, 42.58; H, 4.50; N, 6.41%. Found: C, 42.16; H, 4.40; N, 6.39%. ESI mass spectrometry (methanol) m/z: 729.2, $[C_{31}H_{29}Co_2N_4O_9]^+$; 669.1, $[C_{29}H_{35}Co_2N_4O_7]^+$; 609.1, $[C_{27}H_{31}Co_2N_4O_5]^+$; 305.1, $[C_{27}H_{31}Co_2N_4O_5]^{2+}$. For (acetonitrile) m/z: 729.0 $[C_{31}H_{29}Co_2N_4O_9]^+$; 669.1, $[C_{29}H_{35}Co_2N_4O_7]^+$. FT-IR spectroscopy ($\nu$, cm^{-1}) 1605.0 (m, C═O asym str, acetate); 1442.0 (s, C═O sym str, acetate); 1022.4 (m, O−H); 832.9 (s, P−F str); 767.0 (m, Py-H def); 555.43 (m, P−F). UV−vis spectroscopy (CH_3CN; 0.02 M) λ_{max} = 493 nm (ε = 63.2 L mol^{-1} cm^{-1}). Initially the complex syntheses were conducted under inert atmosphere; however, the complexes were found to be stable in air, and syntheses undertaken under aerobic conditions produced the identical product. Therefore, the syntheses of all cobalt(II) complexes were achieved under aerobic conditions following the same general procedure.

Synthesis of $[Co_2(CO_2EtL2)(CH_3COO)_2](PF_6)$. There was 70% yield. Microanalysis $C_{33}H_{43}Co_2N_4O_9PF_6$ requires: C, 43.91; H 4.80; N, 6.21%. Found: C, 43.21; H, 4.61; N, 6.10%. ESI mass spectrometry (methanol) m/z: 757.36, $[C_{33}H_{43}Co_2N_4O_9]^+$; 729.37, $[C_{32}H_{43}Co_2N_4O_8]^+$. For (acetonitrile) m/z: 757.1, $[C_{33}H_{43}Co_2N_4O_9]^+$. FT-IR spectroscopy ($\nu$, cm^{-1}) 1601.0 (m, C═O asym str, acetate); 1421.0 (s, C═O sym str, acetate); 830.7 (s, P−F str); 762.4 (m, Py-H def); 555.6 (m, P−F). UV−vis spectroscopy (CH_3CN, 0.02 M) λ_{max} = 508 nm (ε = 73.5 L mol^{-1} cm^{-1}).

Synthesis of $[Co_2(CH_3L2)(CH_3COO)_2](PF_6)$. There was 71% yield. Microanalysis $C_{31}H_{41}Co_2N_4O_7PF_6$ requires: C, 44.09; H, 4.89; N, 6.63%. Found: C, 44.09; H, 4.96; N, 6.58%. ESI mass spectrometry (methanol) m/z: 699.2, $[C_{31}H_{41}Co_2N_4O_7]^+$. For (acetonitrile) m/z: 699.1, $[C_{31}H_{41}Co_2N_4O_7]^+$. FT-IR spectroscopy ($\nu$, cm^{-1}): 2925.1 (w, C−H str), 1595.6 (m, C═O asym str, acetate); 1474.7 (m, C═O sym str, acetate); 1422.9 (m, C−H def); 1085.1 (w, C−O str), 829.2 (s P−F str), 555.3 (s, P−F str). UV−vis spectroscopy (CH_3CN, 0.02 M) λ_{max} = 471 nm (ε = 46.2 L mol^{-1} cm^{-1}), λ_{max} = 519 nm (ε = 50.5 L mol^{-1} cm^{-1}).

Synthesis of $[Co_2(BrL2)(CH_3COO)_2](PF_6)$. There was 32% yield. Microanalysis $C_{30}H_{38}Co_2BrN_4O_7PF_6$ requires: C, 39.62; H, 4.21; N, 6.16%. Found: C, 39.35; H, 4.20; N, 6.18%. ESI mass spectrometry (methanol) m/z: 734.99, $[C_{29}H_{38}BrCo_2N_4O_6]^+$. For (acetonitrile) m/z: 765.0 $[C_{30}H_{38}BrCo_2N_4O_7]^+$. FT-IR spectroscopy ($\nu$, cm^{-1}) 2930.7 (m, C−H); 1599.0 (m, C═O asym str, acetate); 1421.3 (s,

dx.doi.org/10.1021/ic302418x | Inorg. Chem. 2013, 52, 2029−2043

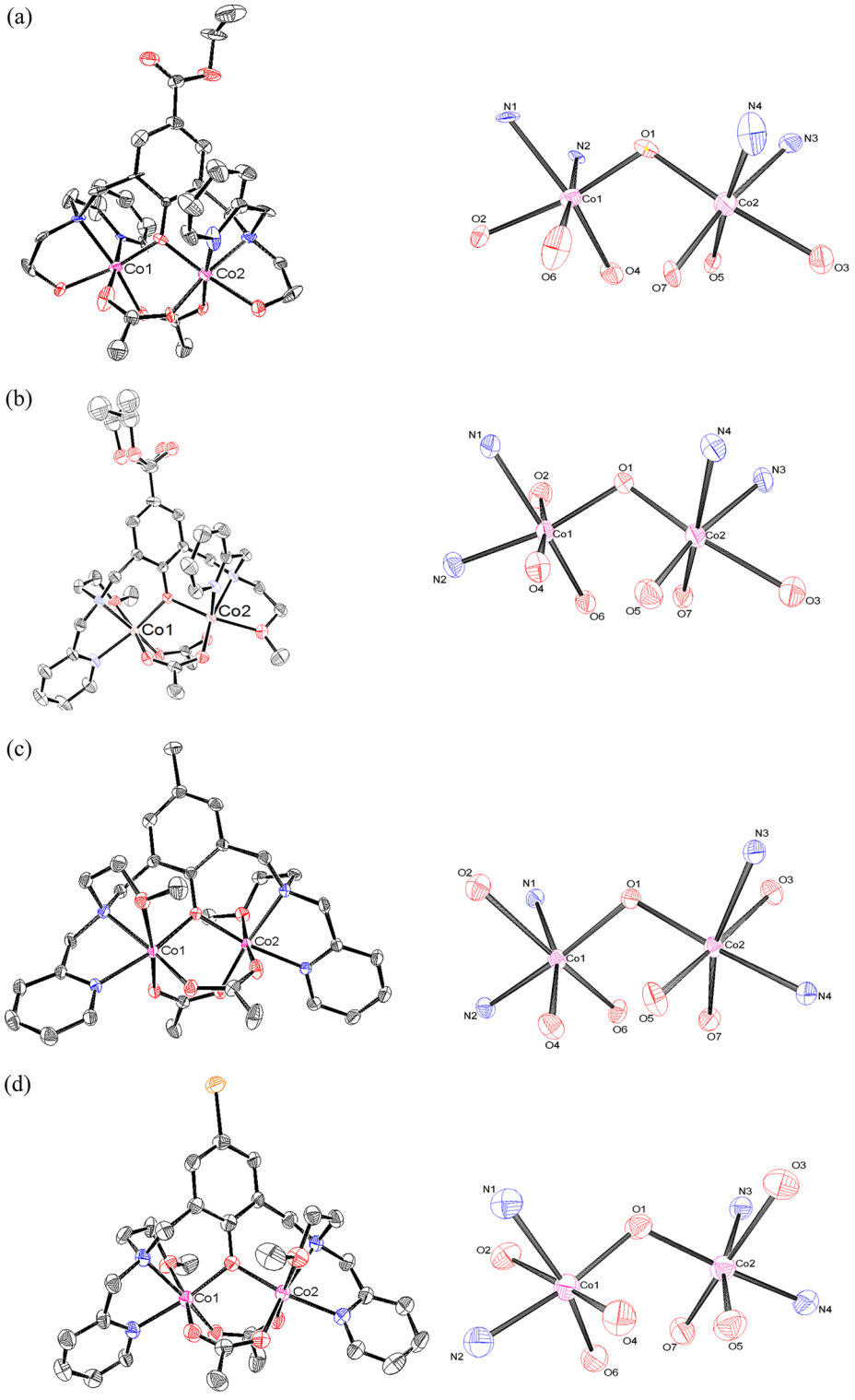

Figure 1. Structures of (a) $[Co_2(CO_2EtH_2\mathbf{L1})(CH_3COO)_2](PF_6)$, (b) $[Co_2(CO_2Et\mathbf{L2})(CH_3COO)_2](PF_6)$, (c) $[Co_2(CH_3\mathbf{L2})(CH_3COO)_2](PF_6)$, and (d) $[Co_2(Br\mathbf{L2})(CH_3COO)_2](PF_6)$ and views of the respective first coordination spheres. Counter ions and hydrogen atoms have been omitted for clarity (25% ellipsoid probability in all ORTEP plots).

C═O sym str, acetate); 831.2 (s, P−F str); 758.8 (m, Py-H def); 555.9 (m, P−F). UV−vis spectroscopy (CH_3CN, 0.01 M) λ_{max} = 460 nm (ε = 4.0 L mol^{-1} cm^{-1}), λ_{max} = 509 nm (ε = 4.1 L mol^{-1} cm^{-1}).

Synthesis of $[Co_2(NO_2L2)(CH_3COO)_2](PF_6).H_2O$. There was 66% yield. Microanalysis $C_{30}H_{40}Co_2N_5O_{10}PF_6$ requires: C, 40.33; H, 4.51; N, 7.84%. Found: C, 40.41; H, 4.42; N, 7.92%. ESI mass spectrometry (methanol) m/z: 784.1, $[C_{30}H_{44}Co_2N_5O_{12}]^+$. For (acetonitrile) m/z: 730.1 $[C_{30}H_{38}Co_2N_5O_9]^+$. FT-IR spectroscopy ($\nu$, cm^{-1}): 2932.7 (w, C−H str); 1594.6 (s, acetate asym str); 1505.7 (w, NO_2 asym str); 1428.6 (s, acetate sym str); 1317.2 (s, NO_2 sym str); 1085.9 (m, C−O str); 829.1 (s, P−F str); 752.3 (m, py C−H def); 657.8 (w, Ar−H def); 555.5 (s, P−F). UV−vis

dx.doi.org/10.1021/ic302418x | Inorg. Chem. 2013, 52, 2029−2043

spectroscopy (CH_3CN, 0.02 M) λ_{max} = 466 nm (ε = 77.7 L mol^{-1} cm^{-1}).

RESULTS AND DISCUSSION

Ligand Nomenclature and Syntheses. The syntheses of the ligands in this study and the nomenclature employed have been described previously and are discussed only briefly here (ligands are shown in Chart 1).[21−23] CO_2EtH_3**L1** denotes that the ligand has an ethyl ester (CO_2Et-) at the position *para*- to the phenolic oxygen and that the ligand has potentially three sites for deprotonation, the phenol and two pendant alcohol donors. Two pyridines and two alcohol arms make up the **L1** donor atom set. The second ligand class, **L2**, offers a direct comparison of methyl ether donors with the alkoxide donor in CO_2EtH_3**L1** and denotes symmetric ligands with two pendant pyridines and two methyl ethers. As only one proton can be potentially subtracted from the **L2** ligands upon deprotonation, the nomenclature is adjusted accordingly. The cobalt(II) complexes were synthesized by adding 2 equiv of cobalt(II) acetate to a methanol solution of the respective ligand (CO_2EtH_3**L1**, CO_2EtH**L2**, CH_3H**L2**, NO_2H**L2**, and BrH**L2**), followed by addition of solid sodium hexafluorophosphate.

Crystal Structures. The complexes $[Co_2(CO_2EtH_2$**L1**$)(CH_3COO)_2](PF_6)$, $[Co_2(CO_2Et$**L2**$)(CH_3COO)_2](PF_6)$, $[Co_2(CH_3$**L2**$)(CH_3COO)_2](PF_6)$, and $[Co_2(Br$**L2**$)(CH_3COO)_2](PF_6)$ were characterized structurally. Selected crystallographic data are shown in Table S1; selected bond lengths and angles are displayed in Table S2. ORTEP plots are shown in Figure 1.[53] The structures comprise the ligand monoanion, two cobalt(II) ions, and two bridging acetates completing the hexacoordinate coordination sphere, with the charge on each complex balanced by a hexafluorophosphate ion. In each case there was disorder around the PF_6^- anion; in addition, $[Co_2(CO_2Et$**L2**$)(CH_3COO)_2](PF_6)$ was found to have significant disorder around the ethyl ester, so the ethyl group was refined in two separate positions. The complexes crystallized in different isomeric forms. Considering that the phenol ring backbone and the two Co(II) ions are in the plane of the page, the ligand arms can be either "in front" of or "behind" the plane. For $[Co_2(CO_2EtH_2$**L1**$)(CH_3COO)_2](PF_6)$ the pyridine nitrogen donors are both *syn*[54] to the phenolic O atom, with pseudo-C_2 symmetry; one pyridine nitrogen donor is in front of, and one is behind, the plane. For $[Co_2(CO_2EtH_2$**L2**$)(CH_3COO)_2](PF_6)$ one pyridine nitrogen donor is *syn* and the other is *anti* with respect to the phenolic O atom. Both $[Co_2(CH_3$**L2**$)(CH_3COO)_2](PF_6)$ and $[Co_2(Br$**L2**$)(CH_3COO)_2](PF_6)$ employ the same coordination geometry as found in the respective zinc complexes, with the pyridine arms *anti*, and an overall pseudo-C_2 symmetry.[54] The overall charge on the complex and the lengths of the metal-to-ligand oxygen donor bonds for $[Co_2(CO_2EtH_2$**L1**$)(CH_3COO)_2](PF_6)$ suggest that the alcohol donors remain protonated. For $[Co_2(CO_2EtH_2$**L1**$)(CH_3COO)_2](PF_6)$, $[Co_2(CO_2Et$**L2**$)(CH_3COO)_2](PF_6)$, $[Co_2(CH_3$**L2**$)(CH_3COO)_2](PF_6)$, and $[Co_2(Br$**L2**$)(CH_3COO)_2](PF_6)$, the coordination environment of both metal ions is composed of the tertiary amine (Co(1)−N(1) 2.168(9), 2.175(4), 2.161(2), 2.172(9) Å; Co(2)−N(3) 2.120(10), 2.154(3), 2.149(3), 2.142(8) Å), the pyridine nitrogen (Co(1)−N(2) 2.145(10), 2.114(4), 2.142(3), 2.111(9) Å; Co(2)−N(4) 2.070(11), 2.182(4), 2.118(2), 2.113(9) Å), the ether oxygens, for $[Co_2(CO_2Et$**L2**$)(CH_3COO)_2](PF_6)$, $[Co_2(CH_3$**L2**$)(CH_3COO)_2](PF_6)$, and $[Co_2(Br$**L2**$)(CH_3COO)_2](PF_6)$ (Co(1)−O(2) 2.235(3), 2.294(3), 2.223(8) Å; Co(2)−O(3) 2.221(3), 2.261(2), 2.266(9) Å), respectively, in addition to the bridging acetates for all complexes. The six coordinate geometry is completed by the bridging oxygen from the phenolate (Co(1)−O(1) 1.992(8), 2.016(3), 2.014(2), 2.014(7) Å; Co(2)−O(1) 2.041(8), 2.044(3), 2.0026(19), 2.009(7) Å) with Co(1)−O(1)−Co(2) 114.6(3)°, 112.25(14)°, 112.81(10)°, and 113.4(3)° and Co(1)−Co(2) distances of 3.394, 3.372, 3.346, and 3.363 Å, respectively. For the complexes with Co(II)−OR ether donors, the bond lengths are in general longer (av 2.253 Å) than for the complexes with Co(II)−O(alkoxide) donors (av 2.195 Å). This finding is in accord with previous studies using a similar complex $[Co_2(bomp)(CH_3COO)_2](BPh_4)$ (Hbomp = 2,6-bis(bis(2-methoxyethyl)aminomethyl)-4-methylphenol), with Co(II)−OR ether donor bonds (av 2.186 Å).[55] For the analogous complex $[Co_2(bhmp)(CH_3COO)_2](BPh_4)$ (Hbhmp = 2,6bis-(bis(2-hydroxyethyl)aminoethyl)aminomethyl)-4-methylphenol), the Co(II)−O alcohol donor bond lengths (av 2.120 Å) are similar to those found for $[Co_2(CO_2EtH_2$**L1**$)(CH_3COO)_2](PF_6)$ (av 2.146 Å).[56] A significant distortion of the coordination sphere around the cobalt centers is apparent in all structures, with the bond distances to the six donor atoms in, for example, $[Co_2(CO_2EtH_2$**L1**$)(CH_3COO)_2](PF_6)$ ranging from 1.989 Å (Co(1)−O(1)) to 2.187 Å (Co(1)−O(6)). The Co(II)−N_{py} distances are similar to those reported for the $[Co_2(L^2)(CH_3COO)_2(MeCN)_2](BPh_4)$ (HL^2 = 2,6-bis(3-pyridin-2-yl)pyrazole-1-ylmethyl]-4-methylphenol) (2.156(5) and 2.178(5) Å).[15] The Co···Co separations are similar to those found for $[Co_2(bhmp)(CH_3COO)_2](BPh_4)$ and $[Co_2(bomp)(CH_3COO)_2](BPh_4)$ (3.356 and 3.336 Å, respectively) and for $[Co_2(L^2)(CH_3COO)_2(MeCN)_2](BPh_4)$ (3.378(5) Å).[15,55,56] The Co(1)−O(1)−Co(2) angles, spanning the phenoxo bridge, do not vary significantly (112.25(14)−114.6(3)°).

A crystal structure of the complex with the ligand NO_2H**L2** could not be obtained despite several attempts. The structure of the complex was subsequently determined from DFT calculations (*vide infra*). The starting parameters for the calculation were those from $[Co_2(CH_3$**L2**$)(CH_3COO)_2](PF_6)$. Geometry optimizations were also conducted for all structures using the Amsterdam Density Functional program and the Becke−Perdew functional.[35] Interestingly, the calculated separation of the cobalt atoms in the complex $[Co_2(NO_2$**L2**$)(CH_3COO)_2](PF_6)$ (3.455 Å) differs significantly from that in the other structures. This value is, however, still in the range reported for the triply bridged μ-oxo-bis(μ_2-CH_3COO-κ^2O:O')cobalt(II) cores.[20] In general, calculated bond lengths and angles are in good agreement with the experimental values (Table S2).

Infrared Spectra. The infrared spectra of all complexes showed a shift of the asymmetric and symmetric acetate stretch to higher frequencies with respect to free acetate (ν_{asym} = 1578 cm^{-1}, ν_{sym} = 1414 cm^{-1}) indicating a bridging bidentate binding mode for the acetate ligands ($[Co_2(CO_2EtH_2$**L1**$)(CH_3COO)_2](PF_6)$, $[Co_2(CO_2Et$**L2**$)(CH_3COO)_2](PF_6)$, $[Co_2(CH_3$**L2**$)(CH_3COO)_2](PF_6)$, $[Co_2(Br$**L2**$)(CH_3COO)_2](PF_6)$, and $[Co_2(NO_2$**L2**$)(CH_3COO)_2](PF_6)$ ν_{asym} = 1605, 1601, 1596, 1599, and 1595 cm^{-1} and ν_{sym} = 1442, 1421, 1424, 1421, and 1429 cm^{-1}, respectively). The magnitude of the separation $\Delta\nu_{asym\text{-}sym}$ confirms a symmetric bidentate coordination for all cobalt complexes in the solid state.[57] The

dx.doi.org/10.1021/ic302418x | Inorg. Chem. 2013, 52, 2029−2043

hexafluorophosphate stretch and deformation bands were found in all spectra around 830 and 555 cm^{-1}, respectively.

Mass Spectral Characterization. Mass spectra were recorded in methanol and acetonitrile solution for all complexes. The spectra measured in methanol revealed the presence of a negatively charged ligand, two cobalt(II) ions, and two acetate ligands for all complexes; fragmentation involving partial loss of the acetate ligands and coordination of methanol solvent molecules was also observed. The mass spectrum of $[Co_2(CO_2EtH_2\mathbf{L1})(CH_3COO)_2](PF_6)$ showed a number of peaks (m/z 729.16, $[Co_2(CO_2EtH_2\mathbf{L1})(CH_3COO)_2]^+$ calcd m/z 729.14; m/z 669.1, $[Co_2(CO_2EtH\mathbf{L1})(CH_3COO)]^+$ calcd m/z 669.12; m/z 609.08, $[Co_2(CO_2Et\mathbf{L1})]^+$ calcd m/z 609.10) in addition to a doubly charged ion (m/z 305.05, $[Co_2(CO_2EtH\mathbf{L1})]^{2+}$ calcd m/z 305.05). The mass spectrum of $[Co_2(CO_2Et\mathbf{L2})(CH_3COO)_2](PF_6)$ showed two fragments with m/z 757.36 and m/z 729.37 assigned to $[Co_2(CO_2Et\mathbf{L2})(CH_3COO)_2]^+$ (calcd m/z 757.17) and $[Co_2(CO_2Et\mathbf{L2})(CH_3COO)(CH_3O)]^+$ (calcd m/z 729.17). The spectrum of $[Co_2(CH_3\mathbf{L2})(CH_3COO)_2](PF_6)$ indicated the formation of $[Co_2(CH_3\mathbf{L2})(CH_3COO)_2]^+$ (found m/z 699.17; calcd m/z 699.16), whereas that of $[Co_2(Br\mathbf{L2})(CH_3COO)_2](PF_6)$ showed a species at m/z 734.99, attributed to $[Co_2(Br\mathbf{L2})(CH_3COO)(CH_3O)]^+$ (calcd m/z 735.06). The mass spectrum of one complex suggested the presence of water ($[Co_2(NO_2\mathbf{L2})(CH_3COO)_2(H_2O)_3]^+$, m/z 784.1; calcd m/z 784.17). The spectra recorded in acetonitrile are shown for all complexes in the Supporting Information (S1–S5). The mass spectrum of $[Co_2(CO_2EtH_2\mathbf{L1})(CH_3COO)_2](PF_6)$ showed similar peaks (m/z = 729.0, 669.1) as those observed in the methanol spectrum in addition to a new doubly charged ion (m/z 335.1, calcd m/z 335.06 $[Co_2(CO_2EtH_2\mathbf{L1})(CH_3COO)]^{2+}$). For $[Co_2(CO_2Et\mathbf{L2})(CH_3COO)_2](PF_6)$ peaks were found at m/z 757.1 and 349.0 (calcd m/z 757.17 and 349.08 for $[Co_2(CO_2Et\mathbf{L2})(CH_3COO)_2]^+$ and $[Co_2(CO_2Et\mathbf{L2})(CH_3COO)]^{2+}$, respectively). Similar species were also found for $[Co_2(CH_3\mathbf{L2})(CH_3COO)_2](PF_6)$ (m/z 699.1 and 320.0, calcd m/z 699.16 and 320.07 for $[Co_2(CH_3\mathbf{L2})(CH_3COO)_2]^+$ and $[Co_2(CH_3\mathbf{L2})(CH_3COO)]^{2+}$, respectively) and $[Co_2(Br\mathbf{L2})(CH_3COO)_2](PF_6)$ (m/z 765.0 and 352.9, calcd m/z 763.06 (100%), 765.06 (99.2%) and 352.02 (100%), 353.02 (97.3%) for $[Co_2(Br\mathbf{L2})(CH_3COO)_2]^+$ and $[Co_2(Br\mathbf{L2})(CH_3COO)]^{2+}$). The latter complex also showed a species at m/z 847.1, which is proposed to arise from additional coordination of two acetonitrile molecules (calcd m/z 845.11 (100%), 847.11 (98.1%) $[Co_2(Br\mathbf{L2})(CH_3COO)_2(MeCN)_2]^+$. The complex $[Co_2(NO_2\mathbf{L2})(CH_3COO)_2](PF_6)$ showed one distinct peak at m/z 730.1 (calcd m/z 730.13, $[Co_2(NO_2\mathbf{L2})(CH_3COO)_2]^+$).

Magnetic Susceptibility Measurements. High-spin octahedral cobalt(II) has a $^4T_{1g}$ ground state. The magnetic moments of complexes with T ground terms are often found to show considerable temperature dependence, and interpreting them is difficult because the occurring angular orbital momentum is partially quenched.[49,55,58−63] Due to large spin−orbit coupling, these systems exhibit substantial zero field splitting, which causes high magnetic anisotropy.

In the solid state the susceptibility data were acquired in the range from 2 to 300 K. Plots of the $\chi_M T$ versus T are illustrated in Figure 2. At 300 K the values of $\chi_M T$ range from 5.49 to 6.29 $cm^3\ mol^{-1}$ K (for the dicobalt(II) complexes) with μ_{eff}/Co = 4.68−5.01 μ_B, larger than the spin-only value expected for a

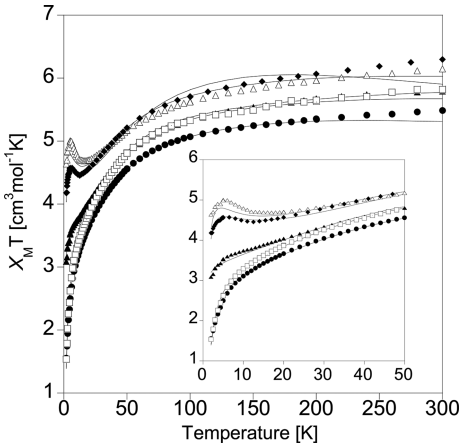

Figure 2. Plot of $\chi_M T$ versus T for powdered samples of the complexes ($[Co_2(CO_2EtH_2\mathbf{L1})(CH_3COO)_2](PF_6)$ = ●, $[Co_2(CO_2Et\mathbf{L2})(CH_3COO)_2](PF_6)$ =▲, $[Co_2(CH_3\mathbf{L2})(CH_3COO)_2](PF_6)$ = □, $[Co_2(Br\mathbf{L2})(CH_3COO)_2](PF_6)$ = ♦, $[Co_2(NO_2\mathbf{L2})(CH_3COO)_2](PF_6)$ = Δ). The solid lines represent the best fit obtained with MagSaki software. Calculated parameters are shown in Table 3. Inset: low temperature data for the complexes.

high spin d^7 ion (S = $^3/_2$, 3.87 μ_B). Including the term for orbital momentum (L = 3) results in an expected magnetic moment of μ_{eff}/Co 5.20 μ_B, which is close to those observed and suggests some quenching of the magnetic moment. All complexes showed significant temperature dependence of the magnetic moment, although upon cooling the behavior of the complexes differs. For $[Co_2(Br\mathbf{L2})(CH_3COO)_2](PF_6)$ and $[Co_2(NO_2\mathbf{L2})(CH_3COO)_2](PF_6)$ the magnitude of $\chi_M T$ decreases smoothly until approximately 12 K and then rises, whereas for $[Co_2(CO_2Et\mathbf{L2})(CH_3COO)_2](PF_6)$, $[Co_2(CH_3\mathbf{L2})(CH_3COO)_2](PF_6)$, and $[Co_2(CO_2EtH_2\mathbf{L1})(CH_3COO)_2](PF_6)$ $\chi_M T$ decreases smoothly to 2 K with values from 1.55 to 3.09 $cm^3\ mol^{-1}$ K, μ_{eff}/Co 2.49−3.51 μ_B. The decrease in the magnitude of $\chi_M T$ with decreasing temperature for these types of complexes has been ascribed to the effect of three factors: the contribution of the orbital angular momentum, intramolecular ferromagnetic coupling, and intermolecular antiferromagnetic coupling.[15,56] The susceptibility data were analyzed using software (MagSaki) that takes the three factors listed above into account and calculates the magnetic susceptibility considering axial distortion, spin−orbit coupling, and anisotropic exchange interaction of two axially distorted octahedral Co(II) centers.[49,60,64] This approach uses the axial-splitting parameter Δ (the splitting of the orbital degeneracy of the $^4T_1$ term by the asymmetric ligand component), an orbital reduction factor κ, the spin−orbit coupling parameter λ, and the magnetic exchange coupling parameter J.[49,60] These variables allow the axial zero field splitting (ZFS) parameter D and anisotropic g-factors to be calculated; the resulting parameters are displayed in Table 1 along with data for similar complexes.[56] Figure 2 shows the experimental data and the fits to the data obtained at 0.5 T. The orbital reduction factor κ for the cobalt(II) complexes is typical for high spin cobalt(II) ions.[62] The κ value for some of the complexes approaches the free ion value (~0.93), and a similar observation is made for the $[Co_2(bhmp)(CH_3COO)_2](BPh_4)$ and $[Co_2(bomp)(CH_3COO)_2](BPh_4)$ complexes.[56] The values of λ are smaller than that reported for the free ion (λ_o = −180 cm^{-1}), but in the range reported for other cobalt(II) complexes; the difference is

dx.doi.org/10.1021/ic302418x | Inorg. Chem. 2013, 52, 2029−2043

Table 1. Magnetic Data for $[Co_2(CO_2EtH_2L1)(CH_3COO)_2](PF_6)$, $[Co_2(CO_2EtL2)(CH_3COO)_2](PF_6)$, $[Co_2(CH_3L2)(CH_3COO)_2](PF_6)$, $[Co_2(BrL2)(CH_3COO)_2](PF_6)$, and $[Co_2(NO_2L2)(CH_3COO)_2](PF_6)$ in Addition to $[Co_2(bhmp)(RCOO)_2](BPh_4)$ and $[Co_2(bomp)(RCOO)_2](BPh_4)$[55,64]

complex	field (Tesla)	J^d (cm^{-1})	λ (cm^{-1})	κ	ν^c	Δ	g_z	g_x	D (cm^{-1})	$R_\chi{}^a$ ($\times 10^{-3}$)	$R_\mu{}^b$ ($\times 10^{-4}$)
$[Co_2(CO_2EtH_2L1)(CH_3COO)_2](PF_6)$	0.5	−0.66	−121	0.72	−4.4	383	2.3	4.7	98	2.2	0.52
	1.0	−0.66	−118	0.70	−3.3	347	2.3	4.7	96	1.9	0.98
$[Co_2(CO_2EtL2)(CH_3COO)_2](PF_6)$	0.5	−0.08	−125	0.93	−5.6	651	2.2	4.9	108	0.61	0.37
	1.0	−0.10	−122	0.93	−5.6	635	2.2	4.9	106	0.67	0.57
$[Co_2(CH_3L2)(CH_3COO)_2](PF_6)$	0.5	−0.67	−112	0.86	−5.0	482	2.2	4.9	98	1.3	0.36
	1.0	−0.68	−108	0.83	−4.9	444	2.2	4.8	94	1.2	0.56
$[Co_2(NO_2L2)(CH_3COO)_2](PF_6)$	0.5	+0.42	−173	0.75	−4.4	571	2.3	4.7	146	5.0	2.4
	1.0	+0.38	−173	0.75	−5.0	649	2.2	4.7	133	4.3	3.3
$[Co_2(BrL2)(CH_3COO)_2](PF_6)$	0.5	+3.13	−102	0.84	−2.4	206	2.9	4.7	135	0.26	0.82
	1.0	+3.19	−102	0.84	−2.3	197	2.9	4.7	137	0.26	0.82
$[Co_2(bhmp)(CH_3COO)_2](BPh_4)$[56,64]	0.5	−0.30	−122	0.80	−6.9	673	2.08	4.74	74	0.033	0.035
$[Co_2(bhmp)(C_6H_5COO)_2](PPh_4)$[56,64]	0.5	−0.21	−99	0.93	−6.0	552	2.15	4.92	69	0.20	0.15
$[Co_2(bomp)(CH_3COO)_2](BPh_4)$[55,94]	0.5	−0.38	−125	0.93	−5.0	581	2.25	4.96	120	0.11	0.91
$[Co_2(bomp)(C_6H_5COO)_2](PPh_4)$[55,64]	0.5	−0.67	−141	0.84	−3.9	461	2.42	4.85	144	1.6	1.5

[a] $R_\chi = \Sigma(\chi_{Acalc} - \chi_{Aobs})^2/\Sigma(\chi_{Aobc})^2$. [b] $R_\mu = \Sigma(\chi_{\mu effcalc} - \chi_{\mu effobs})^2/\Sigma(\chi_{\mu effobs})^2$.[64] [c] Defined as $\nu = \Delta/(\kappa\lambda)$.[56,64] [d] $H = -J_{ex}S_1 \cdot S_2$.

ascribed to covalency effects.[55,56,62,65−67] The ZFS parameter D is typical for six coordinate cobalt(II) complexes and ranges from +95 to +146 cm^{-1}.[55,56,62,65−67] The positive values for the axial splitting parameter Δ (205−651 cm^{-1}) suggest that the axis is elongated and that the orbital singlet is lowest in energy.[68−70] The magnitude of J ($H = -J_{ex}S_1 \cdot S_2$) for $[Co_2(CO_2EtH_2L1)(CH_3COO)_2](PF_6)$, $[Co_2(CO_2EtL2)(CH_3COO)_2](PF_6)$, $[Co_2(CH_3L2)(CH_3COO)_2](PF_6)$, and $[Co_2(NO_2L2)(CH_3COO)_2](PF_6)$ (J = −0.66, −0.10, −0.67, and +0.42 cm^{-1} (0.5 T), respectively) suggests that the intramolecular coupling between the two cobalt(II) sites is extremely weak and is similar to those determined for $[Co_2(bhmp)(CH_3COO)_2](BPh_4)$ and $[Co_2(bomp)(CH_3COO)_2](BPh_4)$ (J = −0.33 to −0.70 cm^{-1}), complexes with a similar ligand μ-phenoxo-bis(μ-acetato) core.[56] For the $[Co_2(BrL2)(CH_3COO)_2](PF_6)$ complex (J = +3.13 cm^{-1}), the situation is less clear. No obvious correlation exists between the magnitude or sign of J and the inductive effects of the differently *para* (NO_2, Br, CO_2Et, and CH_3) substituted complexes.[71]

Attempts have been made to correlate structural parameters with strength of coupling for dicobalt(II) complexes.[20,58,72] Previous suggestions include that the strength of the coupling varies according to bridging type ($O^{2-} > OH^- > H_2O$),[72] that Co(II)−O−Co(II) bond angles around 96° in certain complexes give rise to ferromagnetic coupling through orthogonal magnetic orbitals,[20,67,73] and that bis(μ_2-*syn,syn*-CH_3COO-κ^2O:O') bond angles are important.[15] Tomkowicz et al.[20] reviewed structural parameters for dicobalt(II) complexes with respect to the magnitude of the observed magnetic coupling. One conclusion was that, for complexes with the μ-O_{bridge}/bis(μ_2-RCOO-κ^2O:O') core, the variations in magnetic coupling could be related to the kind of μ-O_{bridge}, the Co−O_{bridge}−Co angle, and the type of R-group.[20] The extent and variation in factors can be further seen in the examples included in Table 2 and Figure S6. It is apparent that extremely weak coupling generally results for complexes with the μ-$O_{(phenoxo)}$;bis(μ_2-CH_3COO-κ^2O:O'), either weakly antiferro- or ferromagnetic, although there are exceptions.[15] Complexes with the μ-H_2O;bis(μ_2-RCOO-κ^2O:O') core appear to promote weak antiferromagnetic coupling, although it is stronger than that seen with the μ-$O_{(phenoxo)}$ analogue. The bis(μ_2-RCOO-κ^2O:O');μ_2-O;κ^2O,O'-CH_3COO core appears to promote ferromagnetic coupling, and the μ-bipym bridge leads to antiferromagnetic coupling. The relationship between Co(II)−X bond distances and the magnitude and sign of J (Figure S6a) is extremely weak, and the Co(II)···Co(II) distance also has no bearing on the coupling (Figure S6b). The extent of distortion around the Co(II) center appears to have little influence; neither the ferromagnetically coupled $[Co_2(\mu$-$CH_3COO)_3(urea)(tmen)_2](OTf)$ (Δ = +80 cm^{-1})[20,74] nor the antiferromagnetically coupled $[Co_2(tidf)(ClO_4)_2(H_2O)_2]$[69] ($\Delta$ = +8.74 cm^{-1}) complexes are substantially distorted from octahedral geometry around the Co(II) sites. Of the structural parameters considered, the Co(II)−X−Co(II) bridge angles appear to have some influence on the sign and magnitude of J (Figure S6c). This observation agrees with those in earlier studies that suggested the importance of the Co−X−Co angle,[20,58,67,73] but unlike coupled dicopper(II)[75,76] and dinickel(II)[77] complexes, the case for a structural relationship for dicobalt(II) complexes is not well resolved.

UV−vis Spectroscopy. UV−vis spectra were recorded for all complexes in solvents employed in the kinetic and MCD studies (acetonitrile and ethanol, respectively). The diffuse reflectance spectra of the complexes as powders were collected as well, and these spectra are shown in Figure S7. The observed transitions for the complexes are listed in Table S3. For all complexes, bands typical for six-coordinate Co(II) were present in solution.[56,78] The UV−vis spectra of $[Co_2(CO_2EtH_2L1)(CH_3COO)_2](PF_6)$ and $[Co_2(CO_2EtL2)(CH_3COO)_2](PF_6)$ in acetonitrile were analyzed. Three transitions were apparent at around 1250, 625, and 450 nm. Gaussian curve analysis suggested that for both complexes the band at around 1250 nm (ν_1; the origin is the $^4T_{1g} \rightarrow {}^4T_{2g}$ transition in O_h symmetry)[78,79] could be simulated by two bands at 1076 and 1257 nm, and at 1073 and 1322 nm, respectively, for $[Co_2(CO_2EtH_2L1)(CH_3COO)_2](PF_6)$ and $[Co_2(CO_2EtL2)(CH_3COO)_2](PF_6)$. These complexes have an octahedral *cis*-CoN_2O_4 geometry at each cobalt(II) site consistent with the splitting of this band into two components under an axial distortion.[55,66,78] Additionally, for each complex the envelope between 750 and 450 nm could be simulated by three bands at 584, 517, and 464 nm,

dx.doi.org/10.1021/ic302418x | Inorg. Chem. 2013, 52, 2029−2043

Table 2. Magnetic Data for Selected Dicobalt(II) Complexes[20,72]

complex	J (cm^{-1})	bridge	Co(II)···Co(II) (Å)	bridge angles (deg)	Co−$X_{(bridge)}$ (Å)
$[Co_2(\mu\text{-}CH_3COO)_3(urea)(tmen)_2](OTf)$[20,74,95]	+18.0[a]	bis(μ_2-CH_3COO-κ^2O:O') μ_2O; κ^2 O,O'-CH_3COO	3.4813	107.7	2.140, 2.1875
$[Co_2(PymPz)_2Cl_4]$[96]	+12.83[a]	di-μ-chlorido	3.551	94.87	2.2825, 2.3723
$[Co_2(PymPz)_2(N_3)_4]$[96]	+10.11[a]	di-μ-azido	3.247	102.38	2.1125, 2.0541
$[Co_2(bta)(H_2O)_6]_n\cdot 2nH_2O$[20,73]	+5.4[b]	μ-H_2O	3.1691	93.89	μ-OH_2, 2.1365, 2.2001
		μ_2O; κ^2 O,O'-RCOO μ_2-RCOO-κ^2O:O'		92.16	μ-O, 2.2506, 2.1478
$[Co_2(L^2)(\mu\text{-}CH_3COO)_2(CH_3CN)_2](BPh_4)$[15]	+2.51[b]	μ-$O_{(phenoxo)}$; bis(μ_2-CH_3COO-κ^2O:O')	3.378	112.83	2.030, 2.024
$[Co(phda)(H_2O)]_n\cdot nH_2O$[20,73]	+2.16[b]	μ-H_2O; μ_2O; κ^2 O,O'-RCOO bis(μ_2-RCOO-κ^2O:O')	3.11499	99.13	2.1222, 2.0948, 2.1440
				93.03	
$[Co_2(BrL2)(\mu\text{-}CH_3COO)_2](PF_6)$	+3.09[b]	μ-$O_{(phenoxo)}$ bis(μ_2-CH_3COO-κ^2O:O')	3.363	113.48	2.013, 2.009
$[Co_2(L^8)_2(\mu\text{-}CH_3COO)_2](BPh_4)_2$[65]	+1.60[b]	bis(μ_2-CH_3COO-κ^2O:O') (*syn/anti* coordination)	4.797		
$[(Co(phen))_2(fum)_2]$[97]	+0.55[a]	bis(μ_2-OOCCHCHCOO-κ^2O:O')	4.464		
$[Co_2(NO_2L2)(\mu\text{-}CH_3COO)_2](PF_6)$	+0.78[b]	μ-$O_{(phenoxo)}$ bis(μ_2-CH_3COO-κ^2O:O')	3.451	112.49	2.078, 2.072
$[Co_2(CO_2EtL2)(\mu\text{-}CH_3COO)_2](PF_6)$	−0.10[b]	μ-$O_{(phenoxo)}$ bis(μ_2-CH_3COO-κ^2O:O')	3.372	112.26	2.016, 2.044
$[Co_2(bhmp)(\mu\text{-}CH_3COO)_2](BPh_4)$[56,64]	−0.37[b]	μ-$O_{(phenoxo)}$ bis(μ_2-CH_3COO-κ^2O:O')	3.3563	112.2	2.027, 2.016
$[Co_2(bomp)(\mu\text{-}CH_3COO)_2](BPh_4)$[56,64]	−0.46[b]	μ-$O_{(phenoxo)}$ bis(μ_2-CH_3COO-κ^2O:O')	3.336	113.02	1.995, 2.005
$[Co_2(CO_2EtL1)(\mu\text{-}CH_3COO)_2](PF_6)$	−0.66[b]	μ-$O_{(phenoxo)}$ bis(μ_2-CH_3COO-κ^2O:O')	3.394	114.55	1.993, 2.041
$[Co_2(CH_3L2)(\mu\text{-}CH_3COO)_2](PF_6)$	−0.67[b]	μ-$O_{(phenoxo)}$ bis(μ_2-CH_3COO-κ^2O:O')	3.346	112.91	2.014, 2.003
$[Co_3(\mu\text{-}CF_3COO)_4(\mu\text{-}H_2O)_2(CF_3COO)_2(H_2O)_2(C_4H_8O_2)]\cdot 2C_4H_8O_2$[98]	−0.4[a]	μ-H_2O bis(μ_2-CF_3COO-κ^2O:O')	3.632	115.1	2.143, 2.160
$[Co_2(\mu\text{-}CH_3COO)(O(N)(O{=}C)_2(CH_2)_3)(Im)_4][OTf]_2$[99]	−1.0[a]	μ_2-CH_3COO-κ^2O:O' μ-$O_{(N\text{-}hydroxyglutarimide)}$	3.6313	126.63	1.9765, 1.977
$[Co_2(\mu\text{-}H_2O)(\mu\text{-}CH_3COO)_2(CH_3COO)_2(phen)_2]$[100]	−2.1[b]	μ-H_2O bis(μ_2-CH_3COO-κ^2O:O')	3.574	114.01	2.134, 2.127
$[Co_2(\mu\text{-}H_2O)(\mu\text{-}CH_3COO)_2(CH_3COO)_2(tmen)_2]$[70]	−1.2[a]	μ-H_2O bis(μ_2-CH_3COO-κ^2O:O')	3.597	115.1	2.147, 2.117
$[Co_2(\mu\text{-}OH_2)(\mu\text{-}CCl_3COO)_2(H_2O)_2(CCl_3COO)_2(IPA)_2]$[20]	−1.5[a]	μ-H_2O bis(μ_2-CCl_3COO-κ^2O:O')	3.642	116.81	2.136, 2.138;
			3.665		2.149, 2.1632
$[Co_2(\mu\text{-}OH_2)(\mu\text{-}CCl_3COO)_2(H_2O)_2(CCl_3COO)_2(DIOX)_2]$[20]	−1.5[a]	μ-H_2O bis(μ_2-CCl_3COO-κ^2O:O')	3.610	115.6	2.124, 2.142
$[Co_2(\mu\text{-}OH_2)(\mu\text{-}Piv)_2(Piv)_2(HPiv)_4]$[20]	−1.6[a]	μ-H_2O bis(μ_2-$C(CH_3)_3COO$-κ^2O:O')	3.430	111.38	2.0800, 2.0983
$[Co_2(Im)_4(CH_3COO)_4(H_2O)]$[72]	−1.6[a]	μ-H_2O bis(μ_2-CH_3COO-κ^2O:O')	3.687	117.2	
$[Co_2(\mu\text{-}OH_2)(\mu\text{-}CCl_3COO)_2(H_2O)_2(CCl_3COO)_2(THF)_2]$[20]	−2.1[a]	μ-H_2O bis(μ_2-CCl_3COO-κ^2O:O')	3.597	115.98	2.120, 2.122;
			3.606		2.133, 2.120
$[Co_2(\mu\text{-}OH_2)(\mu\text{-}CCl_3COO)_2(H_2O)_2(CCl_3COO)_2(glyme)_2]$[20]	−2.1[a]	μ-H_2O bis(μ_2-CCl_3COO-κ^2O:O')	3.594	113.59	2.1479
$[Co_2L_2Cl_2(CH_3OH)_2]$[101]	−4.22[b]	di-μ-$O_{(phenoxo)}$	3.1310	99.461	2.0399, 2.0638
$[Co_2(H_2O)_8(bipym)](SO_4)_2\cdot 2H_2O$[63]	−4.7[b]	μ-bipym	5.782		
$[Co_2(H_2O)_8(bipym)](NO_3)_4$[63]	−5.4[b]	μ-bipym	5.761		
$[Co_2(bipym)_3(H_2O)_4](NO_3)_4\cdot 2H_2O$[62]	−5.4[b]	μ-bipym	5.73		
$[(Co_2(\mu\text{-}OH_2)(\mu\text{-}C(CH_3)_3COO)_2(C(CH_3)_3COO)_2][(\mu\text{-bipym})]_n$[102]	−3[a]	μ-bpym	3.515	108.7	2.168, 2.157
		bis(μ_2-$C(CH_3)_3COO$-κ^2O:O') μ-H_2O	5.587/5.843		
$[Co_2(L^2)(\mu_2\text{-BNPP})_2](ClO_4)\cdot 2CH_3CN$[61]	−3.09[a]	μ-$O_{(phenoxo)}$ bis(μ_2-BNPP-κ^2O:O')	3.667	126.05	2.064, 2.051
$[Co_3(\mu\text{-}CF_3COO)_4(\mu\text{-BA})_2(tmen)_2]$[20,103]	−3.1[a]	μ-$O_{(benzohydroxamate)}$ bis(μ_2-CF_3COO-κ^2O:O')	3.55	118.5	2.054, 2.086
$[Co_2(bipym)_3(NCS)_4]$[63]	−6.2[b]	μ-bipym	5.942		
$[Co_2(\mu\text{-}CH_3COO)_2(AA)(urea)(tmen)_2][OTf]$[95]	−3.6[a]	bis(μ_2-CH_3COO-κ^2O:O') μ-$O_{(acetohydroxamate)}$	3.4316		2.0779, 2.0840
$[Co_2(bpmp)(\mu\text{-}CH_3COO)(CH_3COO)_2]\cdot 3H_2O$[104]	−3.63[a]	μ_2-CH_3COO-κ^2O:O' μ-$O_{(phenoxo)}$	3.462	120.0	1.999
$[Co_2(tidf)(ClO_4)_2(H_2O)_2]$[69]	−10.3[b]	bis-μ-$O_{(phenoxo)}$	3.099	98.15	2.021
$[Co_3(\mu\text{-}CF_3COO)_4(\mu\text{-AA})_2(tmen)_2]$[20,103,105]	−6.4[a]	bis(μ_2-CF_3COO-κ^2O:O') μ-$O_{(acetohydroxamate)}$	3.550	119.31	2.0481, 2.0655
$[Co_2(H_2L^1)_2(MeOH)_2(H_2O)_2]Cl_2\cdot 2MeOH$	−6.9[a]	bis-μ-$O_{(oxime)}$	3.092	96.9	2.055

dx.doi.org/10.1021/ic302418x | *Inorg. Chem.* 2013, 52, 2029−2043

Table 2. continued

complex	J (cm^{-1})	bridge	Co(II)···Co(II) (Å)	bridge angles (deg)	Co−$X_{(bridge)}$ (Å)
$[Co_2(L1)(\mu_2\text{-DPP})](ClO_4)_2{\cdot}0.5CH_3CN{\cdot}0.5C_2H_5OC_2H_5{\cdot}H_2O$[61]	−13.0[a]	μ- $O_{(alkoxo)}$ μ_2-DPP-κ^2O:O'	3.542	127.4	1.974, 1.977

[a] $H = -2J_{ex}S_1{\cdot}S_2$. [b] $H = -J_{ex}S_1{\cdot}S_2$. Å.

and at 570, 515, and 459 nm, respectively, for $[Co_2(CO_2EtH_2\mathbf{L1})(CH_3COO)_2](PF_6)$ and $[Co_2(CO_2Et\mathbf{L2})(CH_3COO)_2](PF_6)$. The highest energy band is assigned to the spin-forbidden transition ($^4T_{1g}\rightarrow{}^2T_{2g}$,$^2T_{1g}$ in O_h symmetry).[56,78] The other two are assigned to spin allowed transitions ν_2 ($^4T_{1g}\rightarrow{}^4A_{2g}$ in O_h) and ν_3 ($^4T_{1g}\rightarrow{}^4T_{1g}$(P) in O_h symmetry), respectively.[56,79,80] On the basis of these assignments, the Racah parameters B (830, 820 cm^{-1}) and D_q (910, 930 cm^{-1}) were determined for $[Co_2(CO_2EtH_2\mathbf{L1})(CH_3COO)_2](PF_6)$ and $[Co_2(CO_2Et\mathbf{L2})(CH_3COO)_2](PF_6)$, respectively.[81] The magnitudes of B and D_q appear typical for these types of complexes.[56,78] Full spectral data for all complexes are reported in Table S3.

Magnetic Circular Dichroism. MCD spectroscopy was used to determine the nature of the magnetic exchange coupling and to explore the coordination geometries of the dicobalt(II) in ethanol solution. The spectra are dominated by temperature-dependent *C*-terms (Figure S8). The MCD intensity above 50 K drops dramatically; thus, no variable-temperature, variable-field (VTVH) data were collected at higher temperatures. Figure S9 displays the field dependence of the spectra for $[Co_2(CO_2Et\mathbf{L2})(CH_3COO)_2](PF_6)$. It is apparent that beyond 5 T the *C*-term intensity is essentially saturated and only the weak field-dependent *B*-term remains. The solid-mull and ethanol-solution MCD spectra for the complexes are shown in Figures S10−16 along with magnetization curves at 1.5, 4.2, and 11.4 K (for the $[Co_2(CH_3\mathbf{L2})(CH_3COO)_2](PF_6)$ and $[Co_2(NO_2\mathbf{L2})(CH_3COO)_2](PF_6)$ complexes, the solid-mull spectra were excessively noisy and are therefore not included). The MCD spectrum of $[Co_2(CH_3\mathbf{L2})(CH_3COO)_2](PF_6)$ is displayed as an example in Figure 3 along with the magnetization curves at 455 and 495 nm. In ethanol, three to four negative bands (~450, 490, 515, 540 nm) dominate the MCD spectra. These bands originate from low symmetry splitting of the $^4T_{1g}\rightarrow{}^4T_{1g}$(P) transition found in high-spin hexacoordinate Co(II). The analysis of VTVH-MCD intensity behavior of the spectra resulted in a series of parameters obtained for a selection of transitions (Table 3). The magnetic data obtained from the MCD suggest weak antiferromagnetic coupling for the $[Co_2(CO_2EtH_2\mathbf{L1})(CH_3COO)_2](PF_6)$, $[Co_2(CO_2Et\mathbf{L2})(CH_3COO)_2](PF_6)$, and $[Co_2(CH_3\mathbf{L2})(CH_3COO)_2](PF_6)$ complexes and ferromagnetic coupling for $[Co_2(NO_2\mathbf{L2})(CH_3COO)_2](PF_6)$ and $[Co_2(Br\mathbf{L2})(CH_3COO)_2](PF_6)$, albeit weak for the former complex, in accord with the results found from the susceptibility measurements.

Angular Overlap Model Calculations. Spectral simulations were made using the angular overlap model (AOM) using the program AOMX essentially as described previously.[19,82,83] Calculations were performed for $[Co_2(CO_2EtH_2\mathbf{L1})(CH_3COO)_2](PF_6)$ and $[Co_2(CO_2Et\mathbf{L2})(CH_3COO)_2](PF_6)$ on the basis of the transitions obtained from the diffuse reflectance and MCD data. The coordinates were generated from the respective crystal structures, and each cobalt(II) metal site was treated separately. The calculations effectively simulated the experimental data for these two complexes; results are listed in Table 4. The Racah parameters C and B were fitted separately, with n in $C = nB$ varying from 4 to 4.7. The Racah B parameter is similar to that determined from the solution spectra, and the e_σ values are as expected in the low range of previously observed parameters;[84] the contribution from π bonding was set to be zero to simplify calculations. The excellent agreement between the AOM

dx.doi.org/10.1021/ic302418x | Inorg. Chem. 2013, 52, 2029−2043

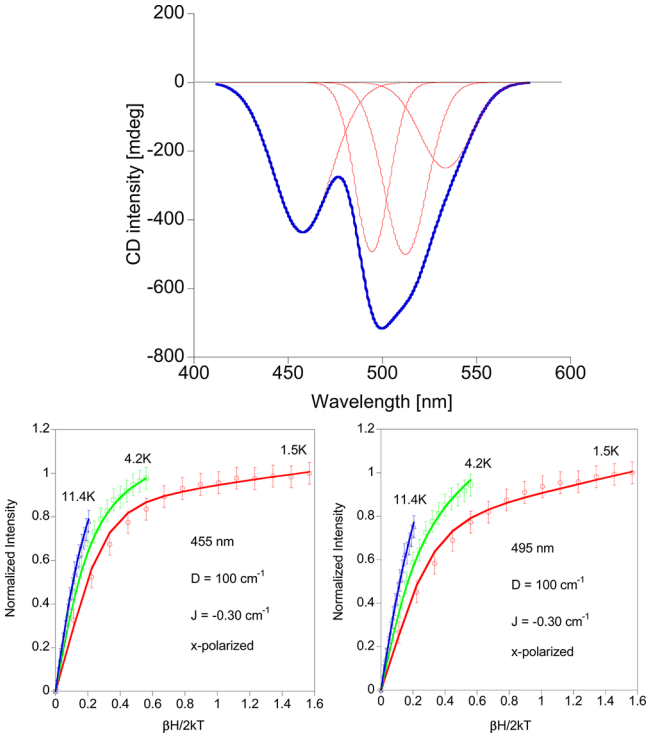

Figure 3. MCD spectrum of $[Co_2(CH_3\mathbf{L2})(CH_3COO)_2](PF_6)$ in ethanol at 1.5 K and 7.0 T (path length 0.62 cm, 34 mM). The experimental spectrum is shown in blue. Gaussian deconvolved spectrum is identical with the recorded spectrum except for noise. Only the Gaussians for the d−d transitions are displayed. On the right: magnetization plots from VTVH analysis of the bands at 455 and 495 nm.

Table 3. Selected Parameters from VTVH MCD

	transition [nm]	J^a [cm^{-1}]	D [cm^{-1}]	%x	%y	%z
		$[Co_2(CO_2EtH_2\mathbf{L1})(CH_3COO)_2](PF_6)$				
mull	530	−0.33	100	97	2	1
mull	506	−0.33	100	84	15	1
EtOH	335	−0.33	100	80	6	14
EtOH	489	−0.34	102	68	27	5
EtOH	510	−0.34	102	43	55	2
		$[Co_2(CO_2Et\mathbf{L2})(CH_3COO)_2](PF_6)$				
EtOH	465	−0.05	108	1	1	99
EtOH	499	−0.05	108	15	0	85
mull	465	−0.10	100	1	0	99
mull	530	−0.10	100	35	0	65
		$[Co_2(CH_3\mathbf{L2})(CH_3COO)_2](PF_6)$				
mull	240	−0.33	98	91	6	3
mull	322	−0.33	98	82	12	6
mull	533	−0.74	98	100	0	0
EtOH	495	−0.30	100	91	1	8
EtOH	455	−0.30	100	93	1	6
		$[Co_2(NO_2\mathbf{L2})(CH_3COO)_2](PF_6)$				
EtOH	480	0.75	100	83	14	3
EtOH	500	0.45	140	96	2	2
EtOH	521	0.75	149	100	0	0
		$[Co_2(Br\mathbf{L2})(CH_3COO)_2](PF_6)$				
EtOH	499	1.5	80	93	0	7
		$[Co_2(Br\mathbf{L2})(CH_3COO)_2](PF_6)$ + DPP				
EtOH	497	0.45	80	92	0	8

$^a H = -2JS_1S2$.

calculated and experimental band positions (Table 4) gives confidence that assigning these bands to d−d transitions is correct and that they are not caused by charge transfer transitions. This idea is further supported by comparing relative intensities of the solution spectra (or diffuse reflectance spectra) with the MCD spectra. Charge transfer bands are relatively intense in absorption spectra and relatively weak in MCD spectra, whereas the opposite is true for d−d transitions.

Electronic Structure Calculations. Our previous computational studies of [Mn(II)Mn(III)] and [Fe(II)Fe(III)] complexes[85,86] have shown that calculations using pure density functionals are able to predict exchange coupling constant (J) values that agree qualitatively with experimental results but that calculated results deviate quantitatively from experimental observations, usually by approximately 20 cm^{-1}. The agreement between experiment and calculation was found to improve significantly, to within approximately 1 cm^{-1}, for calculations using hybrid methods.[85]

The exchange coupling constant was calculated by combining the results for the antiferromagnetic (broken symmetry = BS) and ferromagnetic (high spin = S_{max}) ground state energy, according to eq 3[87,88]

$$E(S_{max}) - E(BS) = -J \cdot {S_{max}}^2 \quad (3)$$

where S_{max} = 3. Results derived from full geometry optimizations (Table 5) are in satisfactory (qualitative) agreement with observations, and the magnitude of quantitative deviation is similar to that reported in previous studies.[85,86] The sole exception is $[Co_2(Br\mathbf{L2})(CH_3COO)_2]^+$, with calculations predicting antiferromagnetic behavior, contrary to experimental observations.

Plots showing the lowest unoccupied level and the five highest occupied levels, with spatial representations of corresponding molecular orbitals, are included in Figure 4 for $[Co_2(NO_2\mathbf{L2})(CH_3COO)_2]^+$ and Figures S17−20, for $[Co_2(CO_2EtH_2\mathbf{L1})(CH_3COO)_2]^+$, $[Co_2(CO_2Et\mathbf{L2})(CH_3COO)_2]^+$, $[Co_2(CH_3\mathbf{L2})(CH_3COO)_2]^+$, and $[Co_2(Br\mathbf{L2})(CH_3COO)_2]^+$. Bonding analysis suggests that, in all five cases, the most important orbital mechanism for interaction between the metal sites involves the phenoxo bridge. As observed in previous studies of [Mn(II)Mn(III)] and [Fe(II)Fe(III)] complexes,[85,86] orbital interactions with combined (M−O) σ-antibonding and π-bonding character are also a common feature of electronic structures across the series of [Co(II)Co(II)] complexes investigated in this work.

The general similarities in relevant aspects of the electronic structures, and the small magnitude of the exchange coupling constants across the series, suggest that relatively small structural differences may be associated with the prediction of ferromagnetic behavior for $[Co_2(NO_2\mathbf{L2})(CH_3COO)_2]^+$, but antiferromagnetic behavior for $[Co_2(CO_2EtH_2\mathbf{L1})(CH_3COO)_2]^+$, $[Co_2(CO_2Et\mathbf{L2})(CH_3COO)_2]^+$, and $[Co_2(CH_3\mathbf{L2})(CH_3COO)_2]^+$. A comparison of calculated geometric parameters (which would be most relevant to structures in solution) for the [M−O−M] bridge indicates that the $[Co_2(NO_2\mathbf{L2})(CH_3COO)_2]^+$ complex exhibits slightly greater [M−M] and [M−O] interatomic distances and a slightly smaller value for the [M−O−M] angle (Table S4).

Computational results for $[Co_2(Br\mathbf{L2})(CH_3COO)_2]^+$, obtained using pure density functionals, indicate that the [M−O−M] bridge structural parameters are, in general, closer to those calculated for $[Co_2(CO_2EtH_2\mathbf{L1})(CH_3COO)_2]^+$, $[Co_2(CO_2Et\mathbf{L2})(CH_3COO)_2]^+$, and $[Co_2(CH_3\mathbf{L2})$-

dx.doi.org/10.1021/ic302418x | Inorg. Chem. 2013, 52, 2029−2043

Table 4. AOMX Calculations for $[Co_2(CO_2EtH_2L1)(CH_3COO)_2](PF_6)$ and $[Co_2(CO_2EtL2)(CH_3COO)_2](PF_6)$

complex[a]	C	B	transition in O_h symmetry[b,c]	obsd [nm]	calcd [nm]	ε_σ N_{tert} [cm^{-1}]	ε_σ N_{py} [cm^{-1}]	ε_σ O_{phenol} [cm^{-1}]	ε_σ O_{Ac} [cm^{-1}]	ε_σ $O_{alcohol/ether}$ [cm^{-1}]
Co(1) $[Co_2(CO_2EtH_2L1)(CH_3COO)_2](PF_6)$	3390	715	$^4T_{1g}\rightarrow{}^4T_{2g}$	1304	1323	4576	5002	4801	3489	726
				1046	992					
			$^4T_{1g}\rightarrow{}^4A_{2g}$	568	588					
			$^4T_{1g}\rightarrow{}^4T_{1g}(P)$	541	539					
				510	503					
				490	489					
			$^4T_{1g}\rightarrow{}^{doublet}$	467	468					
Co(2) $[Co_2(CO_2EtH_2L1)(CH_3COO)_2](PF_6)$	3237	785	$^4T_{1g}\rightarrow{}^4T_{2g}$	1304	1299	3500	3522	4075	3670	999
				1046	1095					
			$^4T_{1g}\rightarrow{}^4A_{2g}$	568	560					
			$^4T_{1g}\rightarrow{}^4T_{1g}(P)$	541	532					
				510	519					
				490	487					
			$^4T_{1g}\rightarrow{}^{doublet}$	467	468					
Co(1) $[Co_2(CO_2EtL2)(CH_3COO)_2](PF_6)$	3309	819	$^4T_{1g}\rightarrow{}^4T_{2g}$	1256	1279	3480	4539	3686	3998	980
				1053	1061					
			$^4T_{1g}\rightarrow{}^4A_{2g}$	546	543					
			$^4T_{1g}\rightarrow{}^4T_{1g}(P)$	518	518					
				500	500					
				465	466					
Co(2) $[Co_2(CO_2EtL2)(CH_3COO)_2](PF_6)$	3319	808	$^4T_{1g}\rightarrow{}^4T_{2g}$	1256	1273	3895	4773	4773	3475	698
				1053	1047					
			$^4T_{1g}\rightarrow{}^4A_{2g}$	546	546					
			$^4T_{1g}\rightarrow{}^4T_{1g}(P)$	518	518					
				500	498					
				465	468					

[a]CoL1A denotes Co(1) from the crystal structure of complex CoL1 and CoL1B stands for Co(2) of this complex. [b]All near IR bands are from the diffuse reflectance spectra. [c]All other bands are taken from the MCD.

Table 5. Computational Parameters ($\Delta E = E_{BS} - E_{S=3}$) for the Calculation of the Magnetic Exchange Coupling via the Broken Symmetry Approach (Equation 3)[a]

complex	ΔE/kJmol^{-1}	J/cm^{-1}
$[Co_2(CO_2EtH_2L1)(CH_3COO)_2]^+$	−1.35	−12.5
$[Co_2(CO_2EtL2)(CH_3COO)_2]^+$	−1.20	−11.1
$[Co_2(CH_3L2)(CH_3COO)_2]^+$	−3.38	−31.4
$[Co_2(NO_2L2)(CH_3COO)_2]^+$	1.90	17.7
$[Co_2(BrL2)(CH_3COO)_2]^+$	−1.88	−17.5

[a]Becke Perdew Functional.

$(CH_3COO)_2]^+$, and antiferromagnetic behavior is also predicted in this case, in contrast to the experimental results. Nevertheless, results derived from single-point calculations involving hybrid methods do show qualitative agreement with experimental observations in the $[Co_2(BrL2)(CH_3COO)_2]^+$ case (Table S5).

Binding of Phosphoesters in Solution. The binding of phosphate esters in solution was investigated by MCD spectroscopy and mass spectrometry. The mass spectrum of $[Co_2(CO_2EtH_2L1)(CH_3COO)_2]^+$ in the presence of 25 equiv of diphenyl phosphate (DPP) is shown in Figure 5. (DPP is a substrate analogue that is not hydrolyzed, because it lacks the activating nitro groups.) The base peak at 1109.2 m/z is proposed to arise from the species $[Co_2(CO_2EtH_2L1)(DPP)_2]^+$ (calcd m/z 1109.17 (100.0%), 1110.18 (56.3%); found m/z 1109.0). The species at m/z 895.0 is assigned to $[Co_2(CO_2EtH_2L1)(DPP)(H_2O)(OH)]^+$ (calcd m/z 895.16 (100.0%), 896.16 (43.1%)). The mass spectrum of $[Co_2(CO_2EtL2)(CH_3COO)_2]^+$ with DPP is shown in Figure S21. The spectrum displays a prominent species assigned to $[Co_2(CO_2EtHL2)(DPP)_2]^+$ (found m/z 1137.0; calcd m/z

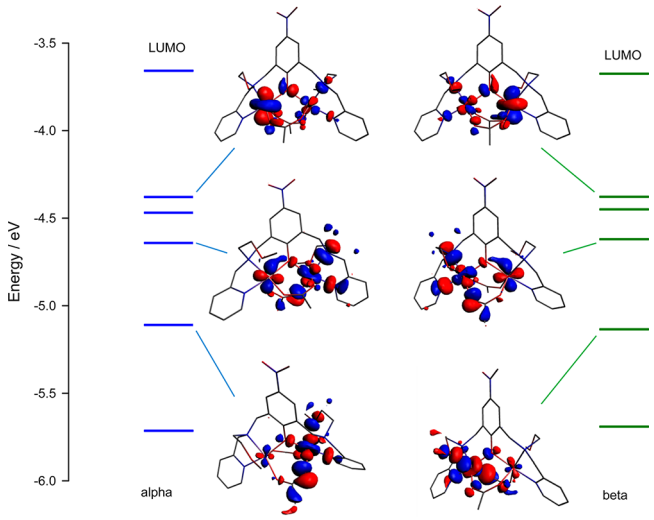

Figure 4. Energy levels and spatial orbital plots for $[Co_2(NO_2L2)(CH_3COO)_2]^+$.

dx.doi.org/10.1021/ic302418x | Inorg. Chem. 2013, 52, 2029−2043

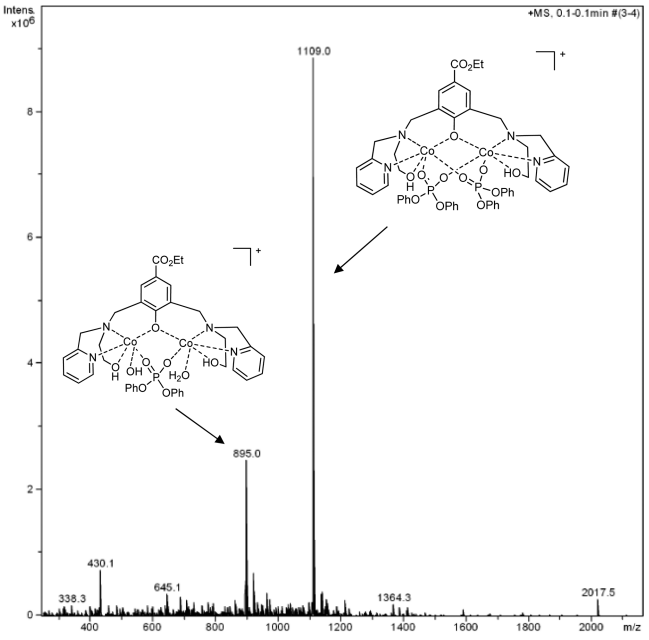

Figure 5. Mass spectrum of $[Co_2(CO_2EtH_2\mathbf{L1})(CH_3COO)_2]^+$ in the presence of 25 equiv of diphenyl phosphate measured in MeCN. $[Co_2(CO_2EtH_2\mathbf{L1})(CH_3COO)_2]^+$ was added to a solution of diphenylphosphate in MeCN (0.01 mM final concentration of complex and 0.25 mM DPP) 10 min prior to spectra recording.

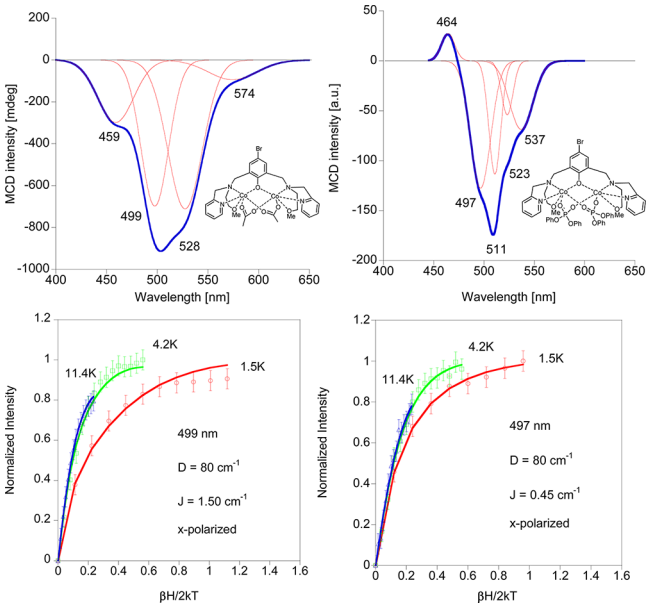

Figure 6. MCD spectra of $[Co_2(Br\mathbf{L2})(CH_3COO)_2]^+$ in ethanol at 1.5 K and 7.0 T (path length 0.62 cm, 10 mM) in the presence and absence of 25 equiv of diphenyl phosphate (DPP). After addition of DPP, the solution was left at room temperature for 12 h prior to recording the spectra. The experimental spectra are shown in blue. Gaussian deconvolved spectra are identical with the recorded spectra except for noise. Left side: $[Co_2(Br\mathbf{L2})(CH_3COO)_2]^+$ in ethanol including magnetization plot of the band at 499 nm below. Right side: $[Co_2(Br\mathbf{L2})(CH_3COO)_2]^+$ + 25 equiv of DPP. Below: magnetization plot from VTVH analysis of the band at 497 nm of the spectrum with DPP present.

1137.21 (100.0%), 1138.21 (58.5%)). In addition, a small peak assigned to $[Co_2(CO_2EtH\mathbf{L2})(DPP)(OH)(CH_3CN)]^+$ is present (found m/z 947.0; calcd m/z 946.20 (100.0%), 947.21 (47.5%)). Figure S22 also shows the mass spectrum of $[Co_2(Br\mathbf{L2})(CH_3COO)_2]^+$ in the presence of 25 equiv of diphenyl phosphate. Only one observed species comprises two cobalt ions, one negatively charged ligand, and two negatively charged diphenylphosphate molecules (found m/z 1144.9, calcd 1143.10 (100%), 1145.09 (97.3%).)

The binding of phosphate esters in solution was also investigated by MCD spectroscopy. Upon addition of 25 equiv of DPP, the spectrum of the complex $[Co_2(Br\mathbf{L2})(CH_3COO)_2]^+$ changes (Figure 6). The intensities and band positions are shifted. VTVH-MCD analysis of the band at ~500 nm revealed that the system is still ferromagnetically coupled in the presence of DPP; however, the coupling constant (0.45 cm^{-1}) drops to one-third of the original value (1.5 cm^{-1}). The Co(II) ions are still hexacoordinate, and mass spectral analysis revealed that two DPP molecules are bound simultaneously. The $[Co_2(Br\mathbf{L2})(CH_3COO)_2](PF_6)$ complex was chosen for the MCD experiments because its spectrum has a better signal-to-noise ratio in ethanol than the other complexes do.

Phosphoesterase Activity. There are surprisingly few comparative studies of cobalt(II) complexes as phosphoesterase mimics.[10−15] For the complexes in the present study the activity toward organophosphoesters using BDNPP, a commonly used model substrate, was investigated. [Substrate] dependence was measured at the pH with highest activity for each complex and followed Michaelis−Menten-type saturation behavior. [Complex] dependence was linear from 0 to 0.12 mM. The data were fitted to an equation derived for a monoprotic system,[32] and the results are shown in Figures 7, 8, and 9 and Table 6. All complexes are good functional mimics for phosphodiesterases and show one relevant pK_a. For the complexes with the methyl-ether donor, the absence of an alkoxide nucleophile and the kinetically relevant pK_a in the range 8.12−8.75 suggests that a terminal water molecule bound to cobalt(II) is the active nucleophile.[21,22] For $[Co_2(CO_2EtH_2\mathbf{L1})(CH_3COO)_2](PF_6)$, fitting of the data resulted in a pK_a of 10.54. For this complex, as with previous studies with this type of ligand,[21,22,29] the possibility exists that the alkoxide may be the active nucleophile. Previous studies have suggested that the coordinated alcohol is deprotonated at or below the same pH as a coordinated water molecule[89] and that a coordinated alcohol is a stronger nucleophile than a coordinated hydroxide.[90,91] However, the pK_a of 10.5 for this complex is still in the range of that for Co(II)−OH_2,[92] and hence the identity of the nucleophile is uncertain. What is apparent is that the activity of the dicobalt(II) complexes toward the substrate BDNPP is similar to that displayed by the analogous dizinc(II) complexes[21] although it does not approach the efficiency of $Co(II)_2$−GpdQ (k_{cat} = 1.62 s^{-1}, k_{cat}/K_m = 1.16 mM^{-1} s^{-1}).[25,27,93]

CONCLUSION

The cobalt(II) complexes of five previously reported phenol-based ligands $CO_2EtH_3\mathbf{L1}$, $CO_2EtH\mathbf{L2}$, $CH_3H\mathbf{L2}$, $BrH\mathbf{L2}$, and $NO_2H\mathbf{L2}$ have been prepared. Attempts have been made to correlate structural parameters with the strength of the magnetic coupling after analyzing the magnetic and spectroscopic properties of the complexes. Computational studies have also been conducted to verify the experimental magnetic coupling constants. Bonding analysis suggests that for all the complexes in this study the most important orbital mechanism for interaction between the metal sites involves the phenoxo

dx.doi.org/10.1021/ic302418x | Inorg. Chem. 2013, 52, 2029−2043

Table 6. Kinetic Parameters Obtained for the Complexes in BDNPP Hydrolysis

complex	pK_a	pH optimum	$k_{cat} \times 10^{-3}$ [s^{-1}]	K_m [mM]	catalytic efficiency k_{cat}/K_m [s^{-1} M^{-1}]
$[Co_2(CO_2EtH_2\mathbf{L1})(CH_3COO)_2]^+$	10.54 ± 0.10	10.70	9.12 ± 0.95	3.26 ± 0.80	2.79
$[Co_2(CO_2Et\mathbf{L2})(CH_3COO)_2]^+$	8.34 ± 0.11	10.40	11.40 ± 1.10	4.31 ± 0.85	2.64
$[Co_2(CH_3\mathbf{L2})(CH_3COO)_2]^+$	8.53 ± 0.11	11.00	5.48 ± 0.63	4.48 ± 1.13	1.22
$[Co_2(Br\mathbf{L2})(CH_3COO)_2]^+$	8.75 ± 0.12	10.00	19.10 ± 4.15	4.62 ± 1.62	4.13
$[Co_2(NO_2\mathbf{L2})(CH_3COO)_2]^+$	8.12 ± 0.12	9.55	9.23 ± 1.65	6.83 ± 2.48	1.35

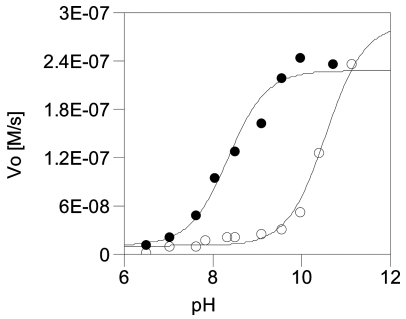

Figure 7. pH dependence profiles for $[Co_2(CO_2EtH_2\mathbf{L1})(CH_3COO)_2](PF_6)$ (o) and $[Co_2(CO_2Et\mathbf{L2})(CH_3COO)_2](PF_6)$ (●).

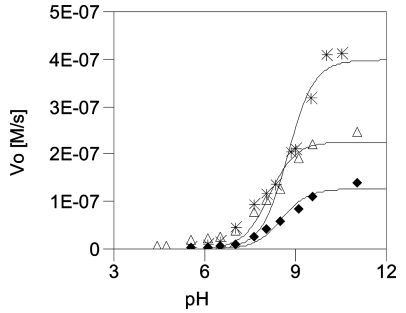

Figure 8. pH dependence profiles for $[Co_2(CH_3\mathbf{L2})(CH_3COO)_2](PF_6)$ (♦), $[Co_2(NO_2\mathbf{L2})(CH_3COO)_2](PF_6)$ (Δ), and $[Co_2(Br\mathbf{L2})(CH_3COO)_2](PF_6)$ (*) shown on the right.

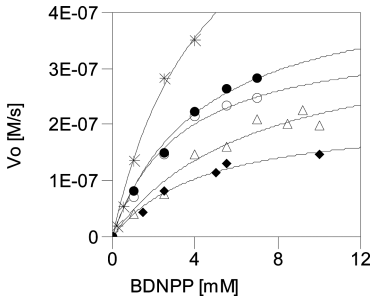

Figure 9. Michaelis–Menten plots for the hydrolysis of BDNPP catalyzed by $[Co_2(CO_2EtH_2\mathbf{L1})(CH_3COO)_2](PF_6)$ (o), $[Co_2(CO_2Et\mathbf{L2})(CH_3COO)_2](PF_6)$ (●), $[Co_2(CH_3\mathbf{L2})(CH_3COO)_2](PF_6)$ (♦), $[Co_2(NO_2\mathbf{L2})(CH_3COO)_2](PF_6)$ (Δ), and $[Co_2(Br\mathbf{L2})(CH_3COO)_2](PF_6)$ (*).

bridge; the differences in magnetic behavior are most likely attributable to minor electronic and structural effects. Mass spectral and MCD studies in the presence of the slow-reacting substrate DPP showed that the complexes can bind up to two substrate molecules and that the geometry of the active site, as well as the magnetic coupling, changes upon substrate binding. Kinetic analysis with the activated substrate BDNPP suggested that, for the complexes derived from **L2** ligands, terminal water is the nucleophile with a kinetically relevant pK_a in the range 8.12–8.75. For the complex with $CO_2EtH_3\mathbf{L1}$, however, the possibility that an alkoxide ligand arm is the active nucleophile cannot be discounted. The complexes in this study are good functional models for enzyme systems.

■ ASSOCIATED CONTENT

Ⓢ Supporting Information

Tables S1 and S2, crystallographic data; Table S3, UV–vis and NIR transitions observed for the complexes; Table S4, comparison of structural parameters for the metal–phenoxo bridge from calculations on broken symmetry states; Table S5, computational parameters for the calculation of the magnetic exchange coupling via the broken symmetry approach. Figures S1–S22. This material is available free of charge via the Internet at http://pubs.acs.org.

■ AUTHOR INFORMATION

Corresponding Author

*E-mail: gahan@uq.edu.au. Phone: +61 7 3365 3844. Fax: +61 7 3365 4299.

Notes

The authors declare no competing financial interest.

■ ACKNOWLEDGMENTS

This work was funded by a grant from the Australian Research Council (DP0986613). L.J.D. was funded by IPRS and UQ graduate school scholarships. Deutscher Akademischer Austausch Dienst (DAAD), the M.G. & R.A. Plowman Scholarship in Inorganic Chemistry (School of Chemistry and Molecular Biosciences, The University of Queensland), and Royal Australian Chemical Institute (RACI) grants awarded to L.J.D. assisted with visits to the University of Heidelberg and Middlebury College for experiments reported in this paper and are gratefully acknowledged. Access to the MagSaki software and advice concerning the fitting of the susceptibility data from Professor Hiroshi Sakiyama from the Department of Material and Biological Chemistry, Faculty of Science, Yamagata University, Kojirakawa, Yamagata, Japan, is greatly appreciated. J.A.L. wishes to acknowledge The National Science Foundation (USA) for financial support from Grant CHE0848433 and Grant CHE0820965 (MCD instrument). The authors are grateful for access to the Australian National University supercomputer facilities of the National Computational Infrastructure.

■ REFERENCES

(1) Wijesekera, R. D.; Sargeson, A. M. *J. Coord. Chem.* **2005**, *58*, 3–19.
(2) Hendry, P.; Sargeson, A. M. *Prog. Inorg. Chem.* **1990**, *38*, 201–258.
(3) Hendry, P.; Sargeson, A. M. *Inorg. Chem.* **1990**, *29*, 92–97.
(4) Fanshawe, R. L.; Blackman, A. G. *Inorg. Chem.* **1995**, *34*, 421–423.

(5) Hettich, R.; Schneider, H.-J. *J. Am. Chem. Soc.* **1997**, *119*, 5638−5647.
(6) Williams, N. H.; Lebuis, A.-M.; Chin, J. *J. Am. Chem. Soc.* **1999**, *121*, 3341−3348.
(7) Seo, J. S.; Sung, N.-D.; Hynes, R. C.; Chin, J. *Inorg. Chem.* **1996**, *35*, 7472−7473.
(8) Hendry, P.; Sargeson, A. M. *J. Am. Chem. Soc.* **1989**, *111*, 2521−2527.
(9) Williams, N. H.; Cheung, W.; Chin, J. *J. Am. Chem. Soc.* **1998**, *120*, 8079−8087.
(10) Brown, R. S.; Zamkanei, M. *Inorg. Chim. Acta* **1985**, *108*, 201−207.
(11) Jikido, R.; Shiraishi, H.; Matsufuji, K.; Ohba, M.; Furutachi, H.; Suzuki, M.; Okawa, H. *Bull. Chem. Soc. Jpn.* **2005**, *78*, 1795−1803.
(12) Zhang, Z.; Yu, X.; Fong, L. K.; Margerum, L. D. *Inorg. Chim. Acta* **2001**, *317*, 72−80.
(13) Lei, G.; Xe, J.; Li, C.; Zhu, J.; Li, J. *Huaxue Yanjiu Yu Yingyong* **2005**, *17*, 200−204.
(14) Zhang, Z.; Xie, J.-q.; Tang, Y.; Li, J.; Li, J.-z.; Zeng, W.; Hu, C.-w. *J. Chem. Res.* **2005**, *2*, 130−134.
(15) Arora, H.; Barman, S. K.; Lloret, F.; Mukherjee, R. *Inorg. Chem.* **2012**, *51*, 5539−5553.
(16) Vallee, B. L. *Cobalt as Probe and Label of Proteins*; Academic Press: New York, 1993; Vol. *226*, pp 52−71.
(17) Solomon, E. I. *Inorganic Chemistry* **2001**, *40*, 3656−3669.
(18) Hadler, K. S.; Mitić, N.; Yip, S. H.-C.; Gahan, L. R.; Ollis, D. L.; Schenk, G.; Larrabee, J. A. *Inorg. Chem.* **2010**, *49*, 2727−2734.
(19) Ely, E.; Hadler, K. S.; Mitić, N.; Gahan, L. R.; Ollis, D. L.; Plugis, N. M.; Russo, M. T.; Larrabee, J. A.; Schenk, G. *JBIC, J. Biol. Inorg. Chem.* **2011**, *16*, 777−787.
(20) Tomkowicz, Z.; Ostrovsky, S.; Foro, S.; Calvo-Perez, V.; Haase, W. *Inorg. Chem.* **2012**, *51*, 6046−6055.
(21) Daumann, L. J.; Dalle, K. E.; Schenk, G.; McGeary, R. P.; Bernhardt, P. V.; Ollis, D. L.; Gahan, L. R. *Dalton Trans.* **2012**, *41*, 1695−1708.
(22) Daumann, L. J.; Gahan, L. R.; Comba, P.; Schenk, G. *Inorg. Chem.* **2012**, *51*, 7669−7681.
(23) Dalle, K. E.; Daumann, L. J.; Schenk, G.; McGeary, R. P.; Hanton, L. R.; Gahan, L. R. *Polyhedron* **2012**, http://dx.doi.org/10.1016/j.poly.2012.06.008.
(24) Raushel, F. M. *Curr. Opin. Microbiol.* **2002**, *5*, 288−295.
(25) Hadler, K. S.; Tanifum, E. A.; Yip, S. H.-C.; Mitić, N.; Guddat, L. W.; Jackson, C. J.; Gahan, L. R.; Nguyen, K.; Carr, P. D.; Ollis, D. L.; Hengge, A. C.; Larrabee, J. A.; Schenk, G. *J. Am. Chem. Soc.* **2008**, *130*, 14129−14138.
(26) Jackson, C. J.; Hadler, K. S.; Carr, P. D.; Oakley, A. J.; Yip, S. H.-C.; Schenk, G.; Ollis, D. L. *Acta Crystallogr.* **2008**, *F64*, 681−685.
(27) Hadler, K.; Mitić, N.; Ely, F.; Hanson, G.; Gahan, L.; Larrabee, J.; Ollis, D.; Schenk, G. *J. Am. Chem. Soc.* **2009**, *131*, 11900−11908.
(28) Hadler, K. S.; Gahan, L. R.; Ollis, D. L.; Schenk, G. *J. Inorg. Biochem.* **2010**, *104*, 211−213.
(29) Chen, J.; Wang, X.; Zhu, Y.; Lin, J.; Yang, X.; Li, Y.; Lu, Y.; Guo, Z. *Inorg. Chem.* **2005**, *44*, 3422−3430.
(30) Batista, S. C.; Neves, A.; Bortoluzzi, A. J.; Vencato, I.; Peralta, R. A.; Szpoganicz, B.; Aires, V. V. E.; Terenzi, H.; Severino, P. C. *Inorg. Chem. Commun.* **2003**, *6*, 1161−1165.
(31) Kaminskaia, N. V.; Spingler, B.; Lippard, S. J. *J. Am. Chem. Soc.* **2000**, *122*, 6411−6422.
(32) Segel, I. H. *Enzyme Kinetics: Behavior and Analysis of Rapid Equilibrium and Steady State Enzyme Systems*, 2nd ed.; Wiley-Interscience: New York, 1975.
(33) *Amsterdam Density Functional, Scientific Computing and Modelling, Theoretical Chemistry*; Vrije University: Amsterdam, The Netherlands (http://www.scm.com).
(34) Fonseca Guerra, S. J. A.; Snijders, T.; Te Velde, G.; Baerends, E. J. *Theor. Chim. Acta* **1998**, *99*, 391−403.
(35) te Velde, G.; Bickelhaupt, F. M.; Baerends, E. J.; Fonseca Guerra, S. J. A.; van Gisbergen, J. G.; Snijders, T.; Ziegler, T. *J. Comput. Chem.* **2001**, *22*, 931−967.
(36) Becke, A. D. *Phys. Rev. A* **1988**, *38*, 3098−3100.
(37) Perdew, J. P. *Phys. Rev. B* **1986**, *33*, 8822−8824.
(38) Becke, A. D. *J. Chem. Phys.* **1993**, *98*, 5648−5652.
(39) Lee, C.; Yang, W.; Parr, R. G. *Phys. Rev. B* **1988**, *37*, 785−789.
(40) Stephens, P. J.; Devlin, F. J.; Chabalowski, C. F.; Frisch, M. J. *J. Phys. Chem.* **1994**, *98*, 11623−11627.
(41) van Lenthe, E.; Baerends, E. J. *J. Comput. Chem.* **2003**, *24*, 1142−1156.
(42) van Lenthe, E.; Baerends, E. J.; Snijders, J. G. *J. Chem. Phys.* **1993**, *99*, 4597−4610.
(43) van Lenthe, E.; Baerends, E. J.; Snijders, J. G. *J. Chem. Phys.* **1994**, *101*, 9783−9792.
(44) van Lenthe, E.; Ehlers, A. E.; Baerends, E. J. *J. Chem. Phys.* **1999**, *110*, 8943−8953.
(45) Pye, C. C.; Ziegler, T. *Theor. Chem. Acc.* **1999**, *101*, 396−408.
(46) Sheldrick, G. M. *SHELXL97: Program for the Refinement of Crystal Structures*; University of Gottingen: Gottingen, Germany, 1997.
(47) Farrugia, L. J. *J. Appl. Crystallogr.* **1999**, *32*, 837−838.
(48) Bain, G. A.; Berry, J. F. *J. Chem. Educ.* **2008**, *85*, 532−536.
(49) Sakiyama, H. *Inorg. Chim. Acta* **2006**, *359*, 2097−2100.
(50) *Thermo Scientific Grams/A1 9.0 Software*, Version 9.0; Thermo Fisher Scientific, Inc. (www.thermofisher.com).
(51) Riley, M. J. *VTVH 2.1.1 Program for the Simulation and Fitting Variable Temperature−Variable Field MCD Spectra*; The University of Queensland: Brisbane, Australia, 2008.
(52) Paulat, F.; Lehnert, N. *Inorg. Chem.* **2008**, *47*, 4963−4976.
(53) Farrugia, L. J. *J. Appl. Crystallogr.* **1997**, *30*, 565.
(54) Comba, P.; DeIuliis, G. N.; Lawrance, G. A.; Luther, S. M.; Maeder, M.; Nolan, A. L.; Robertson, M. J.; Turner, P. *Dalton Trans.* **2003**, 2188−2193.
(55) Sakiyama, H.; Ito, R.; Kumagai, H.; Inoue, K.; Sakamoto, M.; Nishida, Y.; Yamadsaki, M. *Eur. J. Inorg. Chem.* **2001**, 2027−2032.
(56) Hossain, M.; Yamasaki, M.; Mikuriya, M.; Kuribayashi, A.; Sakiyama, H. *Inorg. Chem.* **2002**, *41*, 4058−4062.
(57) Nakamoto, K. *Infrared and Raman Spectra of Inorganic and Coordination Compounds Part B: Applications in Coordination, Organometallic, and Bioinorganic Chemistry Part B*, 5th ed.; John Wiley & Sons, Inc.: New York, 1997.
(58) Johansson, F. B.; Bond, A. D.; Nielsen, U. G.; Moubaraki, B.; Murray, K. S.; Berry, K. J.; Larrabee, J. A.; McKenzie, C. J. *Inorg. Chem.* **2008**, *47*, 5079−5092.
(59) Ostrovsky, S. M.; Werner, R.; Brown, D. A.; Haase, W. *Chem. Phys. Lett.* **2002**, *353*, 290−294.
(60) Sakiyama, H. *J. Chem. Educ., Software* **2001**, *7*, 171−178.
(61) Tian, J.-L.; Gu, W.; Yan, S.-P.; KLiao, D.-Z.; Jiang, Z.-H. *Z. Anorg. Allg. Chem.* **2008**, *634*, 1775−1779.
(62) Lloret, F.; Julve, M.; Cano, J.; Ruiz-Garcia, R.; Pardo, E. *Inorg. Chim. Acta* **2008**, *361*, 3432−3445.
(63) De Munno, G.; Julve, M.; Lloret, F.; Faus, J.; Caneschi, A. *J. Chem. Soc., Dalton Trans.* **1994**, 1175−1183.
(64) Sakiyama, H. *J. Comput. Chem., Jpn.* **2007**, *6*, 123−134.
(65) Mishra, V.; Lloret, F.; Mukherjee, R. *Inorg. Chim. Acta* **2006**, *359*, 4053−4062.
(66) Fabelo, O.; Pasan, J.; Lloret, F.; Julve, M.; Ruiz-Perez, C. *CrystEngComm* **2007**, *9*, 815−827.
(67) Tudor, V.; Marin, G.; Lloret, F.; Kravtsov, V. C.; Simonov, Y. A.; Julve, M.; Andruh, M. *Inorg. Chim. Acta* **2008**, *361*, 3446−3452.
(68) Ostrovsky, S.; Tomkowicz, Z.; Haase, W. *Coord. Chem. Rev.* **2009**, *253*, 2363−2375.
(69) Samulewski, R. B.; da Rocha, J. C.; Fuganti, O.; Stieler, R.; Lang, E. S.; Vaz, M. G. F.; Nunes, F. S. *J. Mol. Struct.* **2010**, *984*, 354−358.
(70) Ostrovsky, S.; Tomkowicz, Z.; Haase, W. *Inorg. Chem.* **2010**, *49*, 6942−6947.
(71) Simon-Manso, Y. *J. Phys. Chem. A* **2005**, *109*, 2006−2011.
(72) Schultz, B. E.; Ye, B.-H.; Li, X.-y.; Chan, S. I. *Inorg. Chem.* **1997**, *36*, 2617−2622.
(73) Fabelo, O.; Canadillas-Delgado, L.; Pasan, J.; Delgado, F. S.; Lloret, F.; Cano, J.; Julve, M.; Ruiz-Perez, C. *Inorg. Chem.* **2009**, *48*, 11342−11351.

(74) Ostrovsky, S.; Falk, K.; Pelikan, J.; Brown, D. A.; Tomkowicz, Z.; Haase, W. *Inorg. Chem.* **2006**, *45*, 688−694.
(75) Crawford, V. H.; Richardson, H. W.; Wasson, J. R.; Hodgson, D. J.; Hatfield, W. E. *Inorg. Chem.* **1976**, *15*, 2107−2110.
(76) Rodriguez-Fortea, A.; Alemany, P.; Alvarez, S.; Ruiz, E. *Chem.—Eur. J.* **2001**, *7*, 627−637.
(77) Bu, X. H.; Du, M.; Zhang, L.; Liao, D. Z.; Tang, J. K.; Zhang, R. H.; Shionoya, M. *J. Chem. Soc., Dalton Trans.* **2001**, 593−598.
(78) Sakiyama, H.; Watanabe, Y.; Ito, R.; Nishida, Y. *Inorg. Chim. Acta* **2004**, *357*, 4309−4312.
(79) Lever, A. B. P.; Ogden, D. *J. Chem. Soc. A* **1967**, 2041−2048.
(80) Herrera, J. M.; Bleuzen, A.; Dromzee, Y.; Julve, M.; Lloret, F.; Verdaguer, M. *Inorg. Chem.* **2003**, *42*, 7052−7059.
(81) Dou, Y.-s. *J. Chem. Educ.* **1990**, *67*, 134.
(82) Adamsky, H.; Schonherr, T.; Artanasov, M. *Comprehensive Coordination Chemistry II*; Elsevier: Oxford, 2004; Vol. *I*.
(83) Schonherr, T.; Atanasov, M.; Adamsky, H. *Comprehensive Coordination Chemistry II*; Elsevier: Oxford, 2004; Vol. *I*.
(84) Bencini, A.; Benelli, C.; Gatteschi, D. *Coord. Chem. Rev.* **1984**, *60*, 131−169.
(85) Smith, S. J.; Peralta, R. A.; Jovito, R.; Horn, A.; Bortoluzzi, A. J.; Noble, C. J.; Hanson, G. R.; Stranger, R.; Jayaratne, V.; Cavigliasso, G.; Gahan, L. R.; Schenk, G.; Nascimento, O. R.; Cavalett, A.; Bortolotto, T.; Razzera, G.; Terenzi, H.; Neves, A.; Riley, M. J. *Inorg. Chem.* **2012**, *51*, 2065−2078.
(86) Smith, S. J.; Riley, M. J.; Noble, C. J.; Hanson, G. R.; Stranger, R.; Jayaratne, V.; Cavigliasso, G.; Schenk, G.; Gahan, L. R. *Inorg. Chem.* **2009**, *48*, 10036−10048.
(87) Delfs, C. D.; Stranger, R. *Inorg. Chem.* **2001**, *40*, 3061−3076.
(88) Noodleman, L. *J. Chem. Phys.* **1981**, *74*, 5737−5743.
(89) Bazzicalupi, C.; Bencini, A.; Berni, E.; Bianchi, A.; Fedi, V.; Fusi, V.; Giorgi, C.; Paoletti, P.; Valtancoli, B. *Inorg. Chem.* **1999**, *38*, 4115−4122.
(90) Li, S. A.; Yang, D. X.; Li, D. F.; Huang, J.; Tang, W. X. *New J. Chem.* **2002**, *26*, 1831−1837.
(91) Xia, J.; Shi, Y. B.; Zhang, Y.; Miao, Q.; Tang, W. X. *Inorg. Chem.* **2003**, *42*, 70−77.
(92) Sillen, L. G.; Martell, A. E., *Stability Constants of Metal-Ion Complexes*; Royal Society of Chemistry: London, 1971; Vol. *25*.
(93) Daumann, L. J.; McCarthy, B. Y.; Hadler, K. S.; Murray, T.; Gahan, L. R.; Larrabee, J. A.; Ollis, D. L.; Schenk, G. *Biochim. Biophys. Acta* **2013**, *1834*, 425−432.
(94) Sakiyama, H.; Ito, R.; Kumagai, H.; Inoue, K.; Sakamoto, M.; Nishida, Y.; Yamasaki, M. *Eur. J. Inorg. Chem.* **2001**, 2705.
(95) Brown, D. A.; Errington, W.; Glass, W. K.; Haase, W.; Kemp, T. J.; Nimir, H.; Ostrovsky, S.; Werner, R. *Inorg. Chem.* **2001**, *40*, 5962−5971.
(96) Jana, A.; Konar, S.; Das, K.; Ray, S.; Golen, J. A.; Rheingold, A. L.; Carrella, L. M.; Rentschler, E.; Mondal, T. K.; Kar, S. K. *Polyhedron* **2012**, *38*, 258−266.
(97) Konar, S.; Zangrando, E.; Drew, M. G. B.; Ribas, J.; Chaudhuri, N. R. *Dalton Trans.* **2004**, 260−266.
(98) Calvo-Perez, V.; Ostrovsky, S.; Vega, A.; Pelikan, J.; Spodine, E.; Haase, W. *Inorg. Chem.* **2006**, *45*, 644−649.
(99) Brown, D. A.; Glass, W. K.; Fitzpatrick, N. J.; Kemp, T. J.; Errington, W.; Clarkson, G. J.; Haase, W.; Karsten, F.; Mahdy, A. H. *Inorg. Chim. Acta* **2004**, *357*, 1411−1436.
(100) Pruchnik, F. P.; Dawid, U.; Kockel, A. *Polyhedron* **2006**, *25*, 3647−3652.
(101) Lin, S.-Y.; Xu, G.-F.; Zhao, L.; Tang, J.; Liu, G.-X. *Z. Anorg. Allg. Chem.* **2011**, *637*, 720−723.
(102) Albores, P.; Rentschler, E. *Dalton Trans.* **2009**, 2609−2615.
(103) Tomkowicz, Z.; Ostrovsky, S.; Muller-Bunz, H.; Hussein Eltmimi, A. J.; Rams, M.; Brown, D. A.; Haase, W. *Inorg. Chem.* **2008**, *47*, 6956−6963.
(104) Huang, C.; Xu, G.; Zhu, H.; Song, Y.; Gou, S. *Inorg. Chim. Acta* **2008**, *361*, 5−8.
(105) Brown, D. A.; Clarkson, G. J.; Fitzpatrick, N. J.; Glass, W. K.; Hussein, A. J.; Kemp, T. J.; Muller-Bunz, H. *Inorg. Chem. Commun.* **2004**, *7*, 495−498.